uOttawa

L'Université canadienne
Canada's university

FACULTÉ DES ÉTUDES SUPÉRIEURES ET POSTOCTORALES

uOttawa

L'Université canadienne
Canada's university

FACULTY OF GRADUATE AND POSDOCTORAL STUDIES

Robert Symonds
AUTEUR DE LA THÈSE / AUTHOR OF THESIS

M.A.Sc. (Chemical Engineering)
GRADE / DEGREE

Department of Chemical Engineering
FACULTÉ, ÉCOLE, DÉPARTEMENT / FACULTY, SCHOOL, DEPARTMENT

CO2 Capture from Gasification Syngas via Cyclic Carbonation/Calcination

TITRE DE LA THÈSE / TITLE OF THESIS

Dr. A. Macchi
DIRECTEUR (DIRECTRICE) DE LA THÈSE / THESIS SUPERVISOR

Dr. Ben Anthony
CO-DIRECTEUR (CO-DIRECTRICE) DE LA THÈSE / THESIS CO-SUPERVISOR

EXAMINATEURS (EXAMINATRICES) DE LA THÈSE / THESIS EXAMINERS

Dr. Poupak Mehrani

Dr. Kevin Kennedi

Gary W. Slater
Le Doyen de la Faculté des études supérieures et postdoctorales / Dean of the Faculty of Graduate and Postdoctoral Studies

CO_2 Capture from Gasification Syngas via Cyclic Carbonation / Calcination

By

Robert Symonds

Thesis submitted to the
Faculty of Graduate and Postdoctoral Studies
In partial fulfillment of the requirements
For the Master of Applied Science in Chemical Engineering

Department of Chemical Engineering
University of Ottawa

Your file Votre référence
ISBN: 978-0-494-48512-5
Our file Notre référence
ISBN: 978-0-494-48512-5

Abstract

Significant research has been carried out to investigate the carbonation of CaO as a potential method for CO_2 capture and sequestration. Up to date, the majority of this work has been related with CO_2 removal from combustion flue gases with little attention focused on the carbonation reaction kinetics under gasification syngas conditions. The intrinsic rate constants of the CaO-CO_2 reaction was studied via a grain model for two naturally occurring calcium oxide based sorbents using a thermogravimetric analyzer. An apparent kinetic model was used to cover both the chemical reaction and diffusion rate control regimes to enable the development of a single phase, plug flow, moving bed carbonator reactor model. Over temperatures ranging from 580-700°C, it was observed that the presence of CO and H_2 during carbonation caused a significant increase in the initial rate of carbonation which has been attributed to the CaO surface sites catalyzing the water-gas shift reaction increasing the local CO_2 concentration. The water-gas shift reaction was assumed to be responsible for the increase the activation energy from 29.7 to 60.3 kJ/mol for limestone and 17.4 to 21.6 kJ/mol for dolomite based on the formation of intermediate complexes. Structural differences between the two sorbents are believed to be accountable for the difference in activation energies. Changes in microporosity due to particle sintering during calcination have been credited with the rapid initial decrease in cyclic CaO maximum conversion for limestone particles whereas the presence of steam during carbonation has been shown to improve the long term maximum conversion in comparison to previous studies without steam present. The dolomite showed a minimal decrease in CaO maximum conversion over repeated cycles as the majority of the carbonation takes place in the larger pores / voids. The effects of major operating parameters such as inlet CaO and feed gas superficial velocities, inlet temperature, and number of calcination / carbonation cycles on the behaviour of the carbonation reaction in a moving bed reactor have been determined. It was revealed that the process is most sensitive to conditions where convective removal of the heat from carbonation is insufficient, limiting the rate of reaction.

Sommaire

Bien de la recherche a été effectuée pour étudier la carbonation du CaO comme méthode potentielle de capture et séquestration du CO_2. Jusqu'à présent, la majorité de ce travail est pour la capture du CO_2 provenant des gaz de combustion avec peu d'attention portée sur la cinétique de la réaction de carbonation avec les gaz de synthèse provenant d'une gazéification. Les constantes cinétiques de la réaction CaO-CO_2 ont donc été étudiées, par l'intermédiaire d'un modèle de grain, pour deux sorbants naturels (chaux et dolomite) à l'aide d'un analyseur thermogravimétrique. Par la suite, un modèle cinétique apparent a été formulé afin de permettre le développement d'un model de réacteur lit mobile. Pour des températures de 580 à 700°C, on a observé que la présence de la CO et du H_2 pendant la carbonation a causé une croissance significative du taux initial de carbonation. Ceci est attribué à la surface de CaO catalysant la réaction eau-gaz (water-gas shift) augmentant ainsi la concentration locale de CO_2. On croit que la réaction eau-gaz est responsable de l'augmentation de l'énergie d'activation de 29.7 à 60.3 kJ/mol pour la chaux et 17.4 à 21.6 kJ/mol pour la dolomite due à la formation de complexes intermédiaires. On pense que des différences structurales entre les deux sorbants sont responsables de la différence entre les énergies d'activation. Une baisse de la microporosité cause une diminution initiale rapide de la conversion maximum cyclique de CaO pour des particules de chaux tandis que la présence de vapeur pendant la carbonation permet d'améliorer la conversion maximum à long terme. La dolomite subie une diminution minimale de conversion maximum cyclique de CaO puisque la majorité de la carbonation a lieu dans les grands pores. Les effets des paramètres d'opération importants tels que les débits et températures d'alimentation de CaO et de gaz, et le nombre des cycles de calcination/carbonation sur le comportement de la réaction de carbonation dans un réacteur lit mobile ont été déterminés. Le procédé est sensible aux conditions où le retrait de l'énergie de la réaction de carbonation est insuffisant, limitant ainsi le taux de réaction.

Table of Contents

List of Tables

List of Figures

Acknowledgements

I would like to first express my gratitude to my supervisors Dr. Macchi and Dr. Anthony for their support, guidance and inspiration and allowing me the opportunity to do a Master's degree.

Secondly, I would like to express my thanks to Dr. Lu and Mr. Hughes for their support during my time at CANMET where I performed my experiments.

Finally, I would like to thank my family and friends who have supported me during my studies.

Chapter 1 – Introduction

The increasing use of fossil fuels to meet energy needs has led to higher CO_2 emissions into the atmosphere. It is widely accepted that, whereas the CO_2 concentration was about 280 ppm before the industrial revolution, it increased from 315 ppmv in 1950 to 355 ppmv in 1990 (Keeling et al., 1989). The rising CO_2 concentration has been reported to account for at least half of the greenhouse effect that causes global warming (Houghton et al., 1996). The need to reduce anthropogenic greenhouse gas emissions represents a major driving force to reconsider the technologies being used for coal combustion and gasification processes (Herzog, 2001). It is apparent that if the rate of fossil fuels consumption is to continue at the current levels, then CO_2 sequestration in deep geological and / or oceanic formations must be employed as a final sink for the CO_2 produced. Geological sequestration involves the pumping of CO_2 into underground coal, oil, and gas fields along with into saline aquifers. There is significant evidence to suggest that these techniques can reliably retain sequestered CO_2 as many high purity naturally formed CO_2 accumulations have been found. Since the ocean is a primary component of the natural carbon cycle, acting as a reservoir to balance atmospheric CO_2 levels, it is thought that by deep ocean release of CO_2 the amount of CO_2 held can be significantly increased.

Current estimates of CO_2 production from fossil fuels are of the order of about 5.4 Gt/a^3 (IPCC, 2005). Although the phenomenon of natural weathering of carbonate rock represents a potential sink on the order of 1 Gt/a^3 this is not sufficient to make a significant impact on CO_2 emissions. At the present time there are several CO_2 separation processes being researched for their deployment in fossil fuel based power plants. These processes include absorption, adsorption, cryogenics, and membrane separation. Absorption processes use chemical solvents such as Selexol, Rectisol, MEA, and KS-2 (Reimer et al., 2001) while adsorption systems use adsorbent materials such as molecular sieves and activated carbon (Kikkinides et al., 1993). Cryogenic systems employ low temperatures to condense out CO_2 from other gases whereas polymers, metals, and molecular sieves are being assessed for the use in membrane based separation processes (Reimer et al., 2001).

For current combustion / gasification systems, one of the only proven commercially available technology to separate CO_2 is based on amine-based absorption systems. Unfortunately, this form of technology introduces harsh efficiency penalties and added costs (Rao and Rubin, 2002). Thus, this justifies a range of emerging approaches that claim to be more energy efficient and cost effective than low-temperature absorption based systems (Abanades et al., 2004). One of the most promising approaches, proposed by Silaban and Harrison (1995), involves the separation of CO_2 at elevated temperatures (>550°C) with a reaction based separation process using a metal oxide such as CaO.

1.1 – Reaction based CO_2 Separation Processes

The essential idea of such a separation approach is to use a sorbent capable of carbonation to remove CO_2 from gasification or combustion effluent streams. This is achieved based on the process in which gaseous CO_2 reacts with a solid metal oxide sorbent to yield a metal carbonate. This reaction (carbonation) can be represented by the following global reaction:

$$M_xO + CO_2 \rightarrow M_xCO_3 \qquad (1.1)$$

Once the metal oxide has reached an appropriate conversion level, it can be thermally regenerated to the metal oxide and CO_2 by heating the metal carbonate beyond the calcination temperature. The calcination reaction can be expressed as follows:

$$M_xCO_3 \rightarrow M_xO + CO_2 \qquad (1.2)$$

There are several advantages associated with a reaction based CO_2 separation process. Firstly, the CO_2 separation can be performed under flue gas (800-1200°C and atmospheric or sub-atmospheric pressure) and syngas (600-1300°C and 1-45 atm) conditions. This has a distinct advantage over such processes as absorption, adsorption, membrane separation, and cryogenics where either low temperatures and/or high pressures are required to increase separation efficiencies. Because typical CO_2

concentrations from fossil fuel fired plants range between 5 and 30%, with the makeup mainly composed of nitrogen, oxygen, and steam, processes that require either cooling or compression of the entire flue gas stream are likely to be expensive (Gupta and Fan, 2002).

Another advantage of reaction based CO_2 separation processes is that metal oxides have high absorption capacities. Under ideal conditions, mono-ethanolamine (MEA) captures 60g of CO_2/kg, silica gel adsorbs 13.2g of CO_2/kg, and activated carbon adsorbs 88g of CO_2/kg (Gupta and Fan, 2002). In contrast, a CaO process would capture 393g of CO_2/kg, assuming a 50% conversion over repeated cycles (Gupta and Fan, 2002). As well, naturally occurring sorbents such as CaO and MgO have very low equilibrium CO_2 concentrations allowing CO_2 in flue gases to be separated to low concentrations.

A final benefit for the use of reaction based CO_2 separation processes is that they can generate a nearly pure stream of CO_2. It is desirable that after regeneration (calcination) the only "off gas" leaving the sorbent / solvent is CO_2. If other gases such as SO_2 or moisture are also evolved from the regeneration step then the process becomes ineffective, as these gases merely concentrate the CO_2 stream failing to produce nearly pure CO_2 (>85 %) needed for sequestration (Kim et al., 2004).

The choice of a suitable metal oxide is critical in determining the viability of the CO_2 separation process. The following table lists the approximate calcination temperatures, at atmospheric pressure, of various metal carbonates that exhibit carbonation and calcination reactions. It is important to note that metal carbonates that decompose (i.e., to a metal oxide and CO_2) at temperatures beyond 1000°C are not considered because their calcination would likely impose severe energy penalties and thermal sintering, which would diminish the reversibility of the reaction.

Table 1.1: Calcination temperature of various metal carbonates (Gupta and Fan, 2002).

	Metal Carbonate					
	$CaCO_3$	$MgCO_3$	$ZnCO_3$	$PbCO_3$	$CuCO_3$	$MnCO_3$
Calcination Temperature (°C)	750	385	340	350	225-290	440

Based on that above calcination temperatures, calcium carbonate in the only suitable cheaply available metal carbonate sorbent based on the exit gas temperature from both combustors and gasifiers. As mentioned above, typical combustor / gasifier

maximum exit temperatures are in the range of 1200 to 1300°C. Thus, having the carbonation reaction taking place at the highest possible temperature will reduce the amount of cooling needed to bring the exit gas to a temperature lower than the sorbent calcination temperature. In turn, this will result in a higher efficiency combined process (combustion or gasification / CO_2 separation).

Up to date there has been significant research on the effect of CO_2 feed gas partial pressures on the reaction kinetics of the CaO-CO_2 reaction (Bhatia and Perlmutter, 1983, Kyaw et al., 1996, and Sun et al., 2008b). These reactions kinetics have been applied to both methane steam reforming (Lee et al., 2004) and water-gas shift (Han and Harrison, 1994) processes utilizing CaO for in-situ CO_2 removal to enhance the production of H_2. Unfortunately, little or no work has been performed on determining if the presence of methane steam reforming feed / product gases (CH_4, H_2O / CO, H_2) or water-gas shift feed / product gases (CO, H_2O / H_2) have an effect on the carbonation reaction kinetics or sorbent deactivation. Thus, the main object of this work is to investigate the effect of gasification syngas on the carbonation kinetics of the gas-solid reaction between CO_2 and CaO for a naturally occurring limestone and dolomite via the use of a grain model which will be discussed in detail in Chapter 3.

1.2 – Gasification Reducing Conditions

Currently hydrogen is produced through three major processes – electrolysis, natural gas reforming, and gasification – the latter of the three being the process most significant to this thesis. Gasification is the production of syngas (mainly CO and H_2) with a significant heating value from a number of carbonaceous fuel sources including coal, petroleum coke, oil, asphaltenes, and biomass. Typically, H_2 is produced from steam which reacts with a solid fuel source at high temperature (1300°C). The overall reaction is as follows:

$$3C + O_2 + H_2O \leftrightarrow 3CO + H_2 \qquad (1.3)$$

The heat for the gasification reaction is supplied through the partial combustion of the feed (sub-stoichiometric oxygen). The exit gas composition is dependant on both

kinetics and equilibrium limitations. After sulphur removal, the syngas can be shifted towards the production of hydrogen via the water-gas shift reaction in the presence of steam. The reaction is as follows:

$$CO + H_2O \leftrightarrow CO_2 + H_2 \quad (1.4)$$

The production of hydrogen via gasification results in the production of large quantities of CO_2 emissions. Thus, the use of gasification as a means for the production of hydrogen must implement significant capture and sequestering of carbon dioxide to be considered an environmentally viable process.

1.3 – Thesis Objectives and Outline

The following goals provide the scope for the present work:

1. Determine the effect of gasification syngas on the carbonation reaction kinetics for naturally occurring calcium oxide based sorbents (limestone and dolomite).
2. Utilization of reaction kinetics for the development of a single phase, plug flow, moving bed carbonator reactor model.
3. Perform sensitivity / parametric analysis of carbonator reactor model.

The thesis outline is as follows: the experimental equipment and measurement techniques are presented in Chapter 2, experimental run conditions and kinetic / moving bed models are developed in Chapter 3, Chapter 4 investigates the effect of operating conditions and sorbent type on carbonation reaction kinetics / sorbent conversion along with a sensitivity analysis of the moving bed reactor model. Finally, conclusions and options for future research are presented in Chapter 5.

Chapter 2 – Experimental Equipment and Measurement Techniques

2.1 – High Pressure Thermogravimetric Analyzer System

Figure 2.1 is a schematic drawing of a high pressure thermogravimetric analyzer system (PTGA). The system is comprised of a hang down tube reactor column made of Inconel 600 alloy with an inner diameter of 0.025 m. Housed within the reactor column is a sample tray (which holds the limestone and dolomite samples) suspended from a Cahn 1000 Electrobalance with 1 μg sensitivity. Gas cylinders containing N_2, CO_2, and a mixed gas (10% CO_2, 25% CO, 50% H_2, and 15% N_2) are mixed at the inlet of the reactor column. Dwyer mass flow controllers (0-100 mL/min) are used to accurately control the gas flow rates to obtain desired feed gas concentrations. Steam is feed to the reactor inlet via a Havard PHD 440 syringe pump and steam generator. Feed lines containing both steam and the mixed gas are insulated and electrically heat traced to ensure no steam condensation. A purge gas (typically N_2 or He) is top feed through the

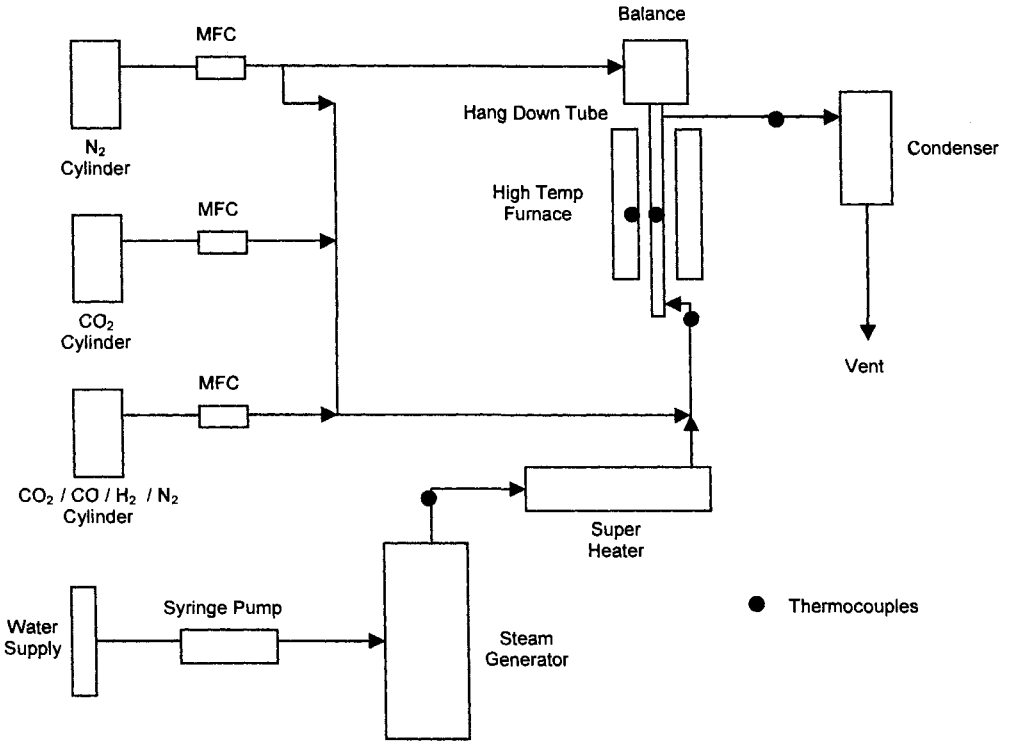

Figure 2.1: Schematic drawing of high pressure thermogravimetric analyzer (PTGA) system.

balance into the reactor column to ensure the sensitive balance electronic components do not overheat and that reaction gases do not enter the balance housing. Outlet gases are subsequently cooled, by passing through a double tube heat exchanger, and vented to the atmosphere. The reactor column is heated by means of an 18 kW LabTemp 16201 electric heater located centrally around the sample tray. System temperatures are monitored using K-type thermocouples located at the steam generator, reactor inlet, sample tray, electric heater, and reactor outlet. Weight measurements are sent from the Cahn 1000 Electrobalance to the control box which is controlled by the use of Labview software. The software is also used to control the gas flow rates, via the mass flow controllers, and the output of the electrically heat traced lines. All temperatures, flow rates, and weight measurements are recorded every 4 seconds and stored in a Microsoft Excel file. All operating conditions such as carbonation periods, gas flow rates, reaction temperatures, etc., will be discussed in detail in Chapter 3.1.

After the limestone / dolomite samples have undergone repeated calcination / carbonation cycles some sample are sent for further analysis. These analyses include visual observation of the sorbent samples via a scanning electron microscope (SEM) and particle pore size distribution / surface area via BET (Brunauer Emmett Teller) analysis. SEM images were taken with a Hitachi S-3400 SEM High Vacuum Mode Imaging machine whereas BET analysis was performed using a Micromeritics ASAP (Accelerated Surface Area and Porosimetry System) 2010 machine.

2.2 – General Measurement Techniques

This section describes the techniques that are used to measure CaO carbonation conversion and sorbent deactivation, via thermogravimetric experiments.

2.2.1 – Sorbent Conversion

Figure 2.2 is an example of a typical CaO / $CaCO_3$ carbonation / calcination experiment using the thermogravimetric analyzer (TGA) system described in Section 2.1 for a natural occurring limestone. In order to determine the CaO carbonation

conversion, X, the following calcium utilization formula can be applied based on a mass basis:

$$X = \frac{m_{CaO}(t) - m_{CaO}(0)}{(purity) \cdot m_{CaCO_3} - m_{CaO}(0)} \tag{2.1}$$

where $m_{CaO}(t)$ and $m_{CaO}(0)$ are the mass of the $CaCO_3$ calcines at a given time t and at the beginning of the carbonation reaction respectively, m_{CaCO_3} is the mass of the fresh sorbent at the start of the run, and *purity* is the mass fraction of $CaCO_3$ of the fresh sorbent at the start of the run. This can be seen more clearly by examining Figure 2.3.

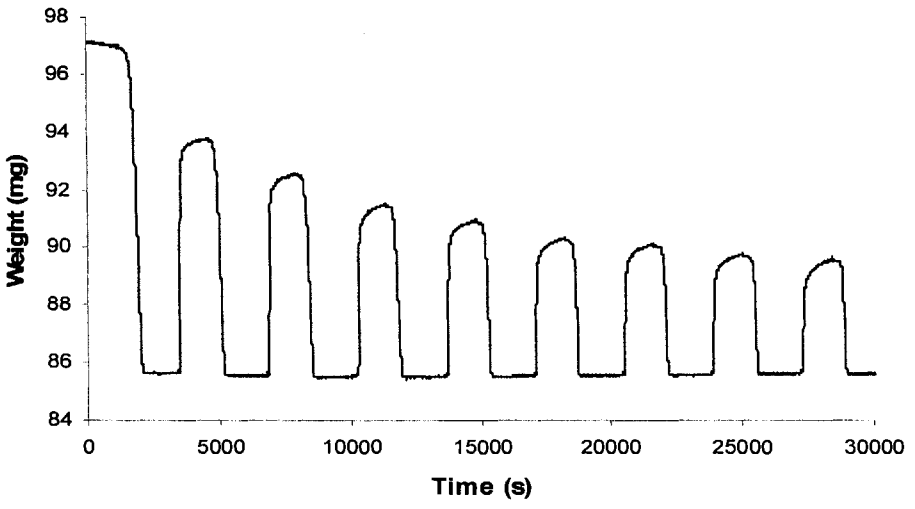

Figure 2.2: Cyclic calcination / carbonation for 250-425 micron Havelock limestone particles calcined at 850°C with N_2 and carbonated at 620°C with 8% CO_2, 21% H_2, 42% CO, 17% H_2O, and 12% N_2.

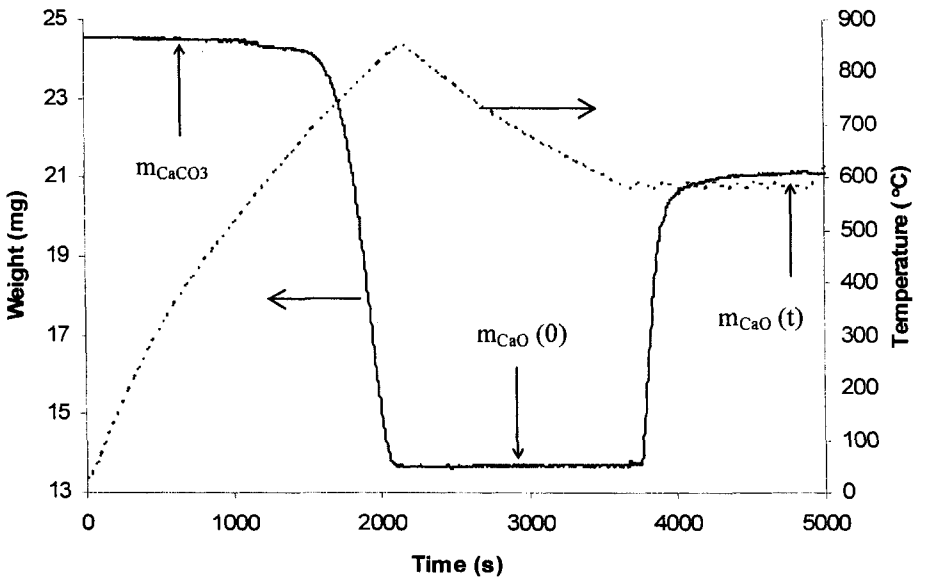

Figure 2.3: First calcination / carbonation cycle for 250-425 micron Havelock limestone particles calcined at 850°C with N_2 and carbonated at 580°C with 8% CO_2, 21% H_2, 42% CO, 17% H_2O, and 12% N_2.

Figure 2.4 is an example of a typical CaO / $CaCO_3$ carbonation / calcination experiment using the thermogravimetric analyzer (TGA) system described in Section 2.1 for a natural occurring dolomite.

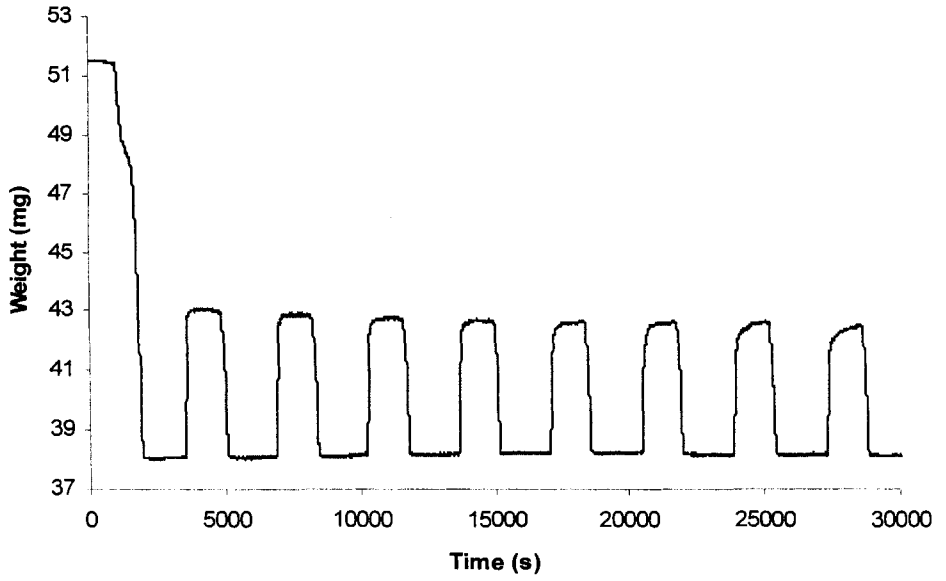

Figure 2.4: Cyclic calcination / carbonation for 250-425 micron Newfoundland dolomite particles calcined at 850°C with N_2 and carbonated at 620°C with 8% CO_2, 21% H_2, 42% CO, 17% H_2O, and 12% N_2.

Unlike most naturally occurring limestones, dolomites contain a significant quantity of $MgCO_3$. Thus, during the initial calcination of dolomite, CO_2 is released from both $MgCO_3$ and $CaCO_3$ but at different temperatures ranges as described in Table 1.1 The initial calcination of dolomite can be seen more clearly by inspection of Figure 2.5. In order to determine the CaO carbonation conversion, the mass fraction of $MgCO_3$ contained within the fresh sorbent must be determined. Although the average $MgCO_3$ content is known (chemical analysis provided by the sorbent distributor), small samples used for TGA experiments show variability in $MgCO_3$ content. It can be seen in Figure 2.6 that the initial percentage change in weight, which is due solely to the calcination of $MgCO_3$, varies from sample to sample under identical calcination conditions indicating an inconsistent mass percentage of $MgCO_3$ contained within fresh dolomite samples. Thus, the mass fraction of $MgCO_3$ must be determined for each individual experimental run sample.

Unfortunately, after the initial rapid change in weight percentage, the calcination of $MgCO_3$ begins to slow down and convolute with the onset of $CaCO_3$ calcination. Therefore, the assumption is made that the calcination of $MgCO_3$ has been completed at the point where the rate of changing weight (indicated by a vertical line in Figure 2.5) is at a minimum. It can be seen that for all three samples in Figure 2.5 the minimum rate of calcination occurs at a temperature of approximately 660°C. It should be noted that this temperature is in agreement with the onset of $CaCO_3$ calcination for naturally occurring limestones as can observed in Figure 2.6. Thus, the CaO carbonation conversion for each cycle can be determined via the following calcium utilization formula applied on a mass basis:

$$X = \frac{m_{CaO}(t) - m_{CaO}(0)}{m_{CaCO_3,CO_2} - m_{CaO}(0)} \tag{2.2}$$

where m_{CaCO_3,CO_2} is the mass of dolomite after complete calcination of $MgCO_3$ or the mass of the sorbent at 660°C calcined under pure N_2.

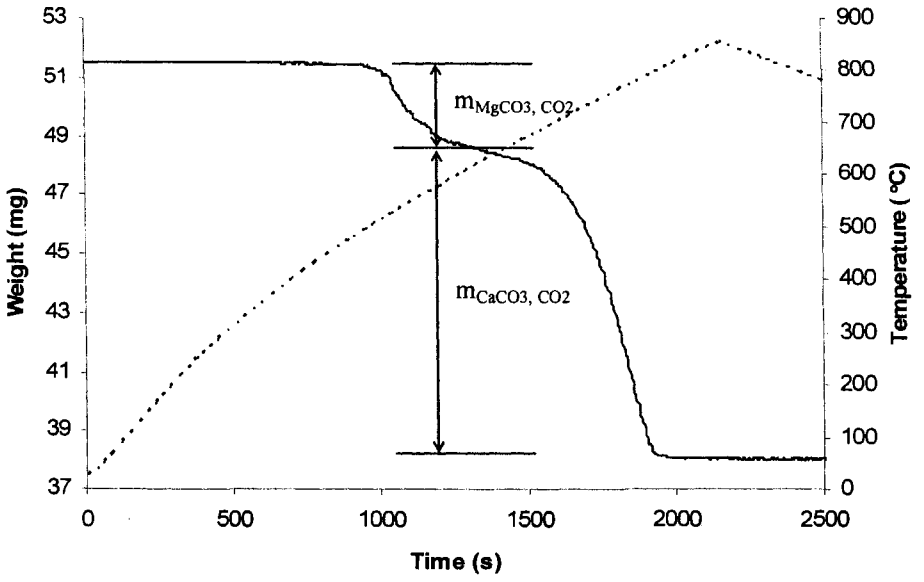

Figure 2.5: Initial calcination for 250-425 micron Newfoundland dolomite particles calcined at 850°C with N_2.

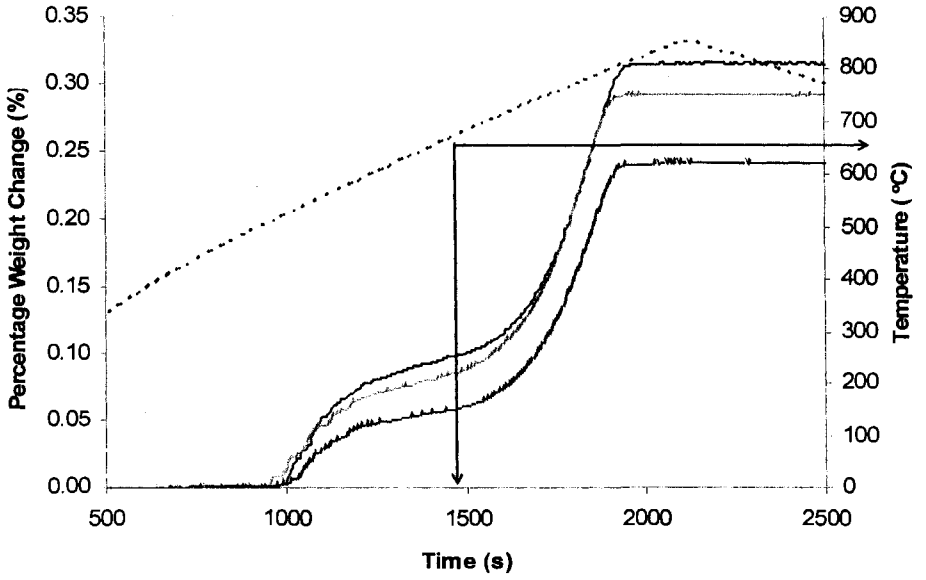

Figure 2.6: Initial calcination for three samples of 250-425 micron Newfoundland dolomite particles calcined at 850°C with N_2.

2.2.2 – Sorbent Deactivation

From the perspective of the solid-sorbent (in this case both naturally occurring limestones and dolomites), it is obvious by examining Figures 2.2 and 2.4 that the samples of CaO achieve a degree of carbonation well below unity over the carbonation time employed here. This limited conversion, $X_{b,N}$, can be determined for each carbonation cycle, N, and sorbent type via the use of Equations 2.1 and 2.2 by substituting in the mass of the $CaCO_3$ calcines at the end of the carbonation period, $m_{CaO,b,N}$:

$$X_{b,N} = \frac{m_{CaO,b,N} - m_{CaO}(0)}{(purity) \cdot m_{CaCO_3} - m_{CaO}(0)} \tag{2.3}$$

$$X_{b,N} = \frac{m_{CaO,b,N} - m_{CaO}(0)}{m_{CaCO_3,CO_2} - m_{CaO}(0)} \tag{2.4}$$

Again by inspection of Figures 2.2 and 2.4, it becomes apparent that the limited conversion decreases with the number of calcination / carbonation cycles. Numerous studies on the reversibility of the carbonation reaction have reported a similar decay in limited conversion over a comparable number of cycles (Abanades and Alvarez, 2003). From these studies a simple model has been developed at the particle level to account for this decay (Abanades and Alvarez, 2003) that translates into the following semi-empirical correlation:

$$X_{b,N} = f_m^N (1 - f_w) + f_w \tag{2.5}$$

where f_m is the fractional loss in sorbent microporosity (or conversion associated with this microporosity) per cycle and f_w is proportional to the product of several factors including the fractional shrinking in sorbent microporosity per cycle, the fraction of the specific surface associated with the void volumes forming the mesoporosity, and the

thickness of the product layer. It should be noted that Equation 2.5 is only applicable to naturally occurring limestones and not dolomites as the surface morphologies of these two sorbents are significantly different (Sun et al., 2008b). A more detailed explanation of the model development and parameter characterization will be discussed in Chapter 4.

Equation 2.5 can be fitted directly to the experimental data, limited conversion and carbonation cycle, so that the optimum values for the two parameters f_m and f_w can be obtained for each experimental condition. This can be achieved by linearization of Equation 2.5 as follows:

$$\ln\left(\frac{X_{b,N}-f_w}{1-f_w}\right)=\ln(f_m)\cdot N \tag{2.6}$$

Due to the nature of the sorbent deactivation model, after linearization both parameters f_m and f_w cannot be explicitly determined. Therefore, the value of f_w must initially be assumed then adjusted via several iterations so that the error (sum of squares) for the line of best fit is minimized. Once the iterative procedure is completed the value of f_m can be determined by utilizing the following formula:

$$f_m = e^s \tag{2.7}$$

where s is the slope of the line of best fit. This can be seen more clearly by inspection of Figure 2.7 which is a plot of $\ln((X_{b,N}-f_w)/(1-f_w))$ versus cycle number, N :

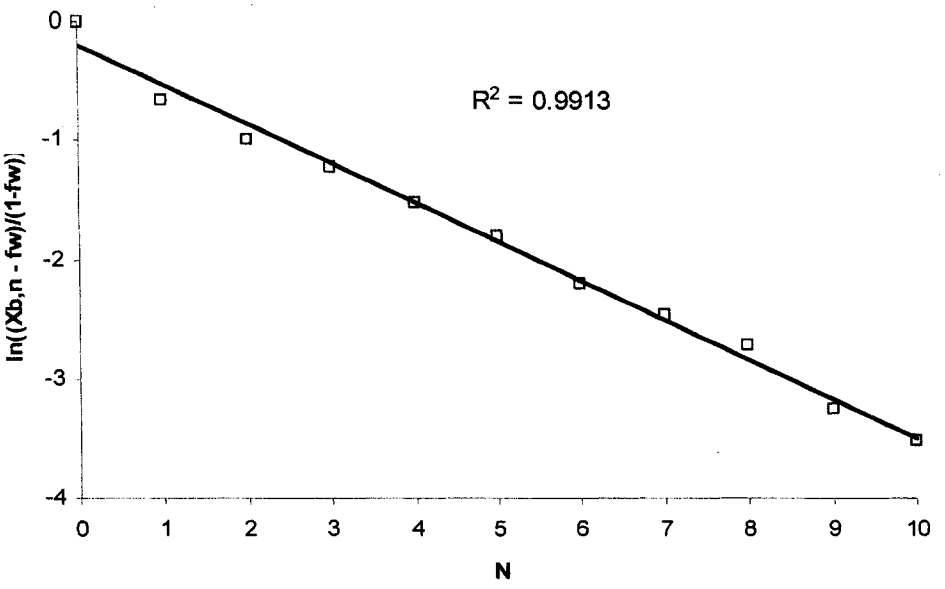

Figure 2.7: Left-hand side of Equation 2.6 versus cycle number for 250-425 micron Havelock limestone particles calcined at 850°C with N_2 and carbonated at 580°C with 8% CO_2, 21% H_2, 42% CO, 17% H_2O, and 12% N_2.

Chapter 3 – Experimental Run Conditions and Kinetic / Moving Bed Models

3.1 – Experimental Run Conditions

As mentioned in Chapter 1.3, the main objective of this thesis is to investigate the effect of gasification syngas on the carbonation kinetics of the gas-solid reaction between CO_2 and CaO. The run conditions include the carbonation of a limestone and dolomite over the temperature range of 580 to 700°C under both syngas and non-syngas conditions. Calcination is performed both under N_2 / N_2 and CO_2 conditions with an associated calcination temperature of 850 and 915°C, respectively. In each case, the system was run under atmospheric pressure for 10 cycles using particles in the size range of 250-425 microns.

The CaO sources for the experiments were a naturally occurring Canadian limestone and dolomite. The limestone, known as Havelock, was selected based on its performance in pilot-scale fluidized-bed reactor testing for CO_2 capture from combustion flue gases at high temperatures (Abanades et al., 2004). Not only did it show a significantly higher cyclic stability than other types of limestones, tested under similar conditions, but it has a relatively low associated cost and is available in significant quantities throughout areas where this technology might be implemented. The dolomite, known as Newfoundland dolomite, was selected for comparison to the limestone based on its reported high cyclic stability while maintaining a reasonable CO_2 capture capacity (Li et al., 2005). For both sorbents, fairly large samples of between 24 and 26 mg were used for TGA experiments to try to avoid any variance in chemical composition between runs as individual particles can display different CaO / MgO ratios. It should be noted that varying the sample size showed no difference in the mass breakthrough profile indicating no "packing" effects causing interparticle mass transfer resistance. Particles in the size range 250-425 micron were used for testing. This size range was used based on two factors. The first is that particles larger than 425 micron have been shown to be affected by intraparticle mass transfer during carbonation (Sun et al., 2008) whereas the use of particles under 250 micron incur large energy penalties due to excessive crushing and grinding. Chemical analyses of these two sorbents, performed via x-ray diffraction

(XRD), are provided in Table 3.1. It should be note that the initial surface areas determined via BET analysis are 16.0 and 12.73 m^2/g for Havelock limestone and Newfoundland dolomite, respectively.

Table 3.1: XRD chemical analysis of Havelock limestone and Newfoundland dolomite (in weight percentage).

Sorbent	SiO_2	Al_2O_3	Fe_2O_3	MgO	CaO	Na_2O	K_2O	LOI
Havelock	1.90	0.34	0.30	0.29	54.10	0.20	0.06	42.99
Newfoundland Dolomite	2.12	0.17	1.30	21.25	30.51	0.15	0.04	44.40

To determine the effect of gasification syngas on the carbonation kinetics, a syngas composition had to be selected for experimentation. The selected composition was based on the exit gas composition of the Chevron-Texaco gasifiers which uses wet Illinois bitumenous coal as a feed (Simbeck et al., 1993). Due to the numerous trace gases found within the effluent of the Chevron-Texaco gasifiers and the limitation in the precision of synthetic mixed gas cylinders, gases such as CH_4, H_2S, and NH_3 + HCN have been omitted from the syngas feed stream. In order to observe the effect of syngas on the carbonation reaction kinetics, experimental runs containing no CO or H_2 (main constituents of syngas) have been performed for comparison. In both cases the CO_2 partial pressure remains constant and the balance is made up of inert N_2. The total gas flow rate was set at 100 standard mL/min for a carbonation period of 20 minutes. Table 3.2 lists the carbonation feed gas compositions for experiments performed with and without the presence of CO and H_2.

Table 3.2: Carbonation feed gas compositions (in volume fraction).

Carbonation Feed Gas	CO_2	CO	H_2	H_2O	N_2
With CO and H_2	0.08	0.42	0.21	0.17	0.12
Without CO and H_2	0.08	0	0	0.17	0.75

As determined by Baker (1962), the equilibrium vapour pressure of CO_2, $P_{CO_2,eq}$, over CaO at a temperature, T, is given by the following expression:

$$\log_{10}(P_{CO_2,eq}) = 7.079 - \frac{8308}{T} \tag{3.1}$$

Based on the above equation, it can be seen that the equilibrium partial pressure of CO_2 increases with increasing temperature. Since the feed gas composition has been set, the equilibrium carbonation temperature is purely a function of the CO_2 partial pressure. Based on the limitations of the experimental apparatus, the experiments in this work have all been conducted at atmospheric pressure. Here, the equilibrium temperature for a CO_2 partial pressure 0.08 atm is approximately 740°C. Thus, the maximum carbonation temperature was set at 700°C in order to have an appropriate CO_2 concentration gradient for the reaction to proceed. The minimum carbonation temperature was set at 580°C, as temperatures lower than this value result in extremely slow rates of carbonation not applicable for effective CO_2 removal from gasification effluent streams. Also, as noted in Chapter 1.1, a typical gasifier outlet temperature is in the range of 1200 to 1300°C. Therefore, significant cooling would be required to bring the flue gas down to carbonation reaction temperature reducing the combined process efficient (gasification / carbonation). Based on the minimum and maximum temperatures, four temperatures were chosen for carbonation runs. These temperatures were 580, 620, 660, and 700°C to provide adequate kinetic data needed for the determination of the carbonation activation energy (see Chapter 3.2).

As will be discussed in Chapter 3.2, the intrinsic carbonation reaction kinetics of the sorbents are quantified via the use of a grain model with kinetic control. The underlining assumption for the use of this model is that the micrograins are spherical. Thus, in order to avoid the initial grain-neck growth resulting in non-spherical micrograins, the partial pressure of CO_2 was set to zero, using only pure N_2 for calcination. With pure N_2, complete calcination was achieved by heating of the sorbent sample from the pre-determined carbonation temperature to 850°C thus, minimizing the effect of time at temperature on particle sintering. The effect of CO_2 and time at temperature during calcination will be discussed in detail in Chapter 4.

From a practical point of view, the use of N_2 (or air) during calcination would negate the point of CO_2 separation since subsequent downstream processing would be required to separate the N_2 (or air) from the CO_2 necessary for sequestration. Thus, in practice, sorbent calcination would likely be carried out using an oxy-fuel fired

combustor (Shimizu et al., 1999) by burning a fraction of the fuel in the calciner with O_2/CO_2. Therefore, preliminary experimental runs have been performed using CO_2 and N_2, simulating oxy-fuel fired calcination conditions, in order to look at the effect of CO_2 sintering on the carbonation of calcium oxide based sorbents. The CO_2 partial pressure was set at 0.90 atm to mimic calcination conditions used by Abanadas et al. (2003). It should be noted that N_2 has been used instead of O_2 due to safety considerations and is assumed to have no enhancement effect on particle sintering. Based on a CO_2 partial pressure of 0.90 atm the associated equilibrium temperature was determined to be approximately 890°C. Thus, to achieve rapid calcination and not incur severe energy penalties, the calcination temperature was set at 915°C and complete decomposition was observed over a 20 minute period.

For each experimental condition, two runs were performed to ensure the repeatability of the data and indicated no more than a 5% relative error between runs. Thus, including repeat tests, a total of 40 experiments were performed.

3.2 – Kinetic Models

It is well understood that the gas-solid chemical reaction between CO_2 and CaO proceeds through two principal rate controlling regimes (Figure 3.1). Initially, the carbonation of CaO proceeds quickly by heterogeneous surface chemical reaction kinetics (Kunii and Levenspiel, 1969). However, during this initial stage a compact product layer of $CaCO_3$ is formed on the outer regions of the CaO particles. This results in a significant decrease in the carbonation reaction rate as the CO_2 molecules must now diffuse through the $CaCO_3$ product layer to access the unreacted CaO.

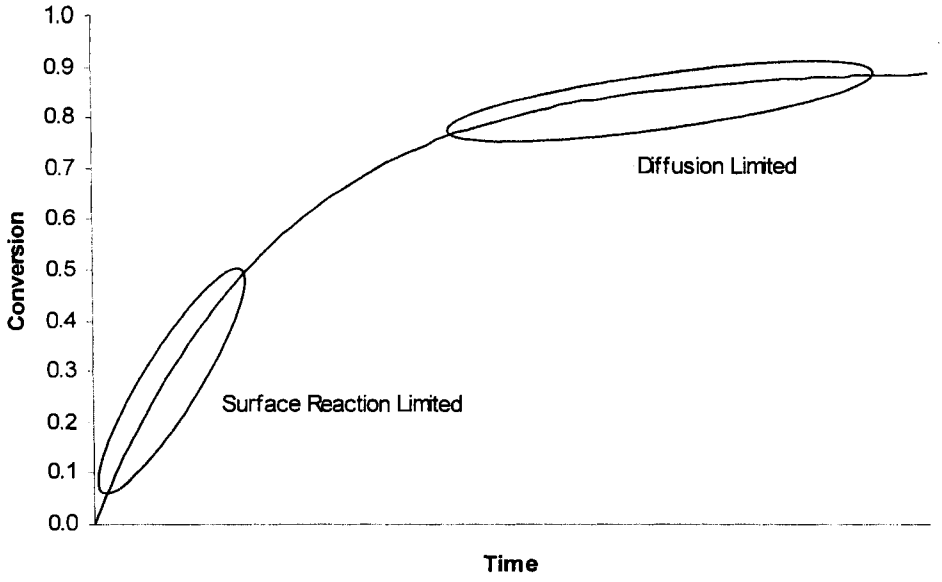

Figure 3.1: Typical behaviour for CaO carbonation - conversion vs. time plot.

Several models have been proposed in order to describe the CO_2 - CaO gas-solid chemical reaction kinetics. The classical models that have been proposed are the continuous and unreacted core models (Kunii and Levenspiel, 1969). Unfortunately, neither of these models are appropriate to represent CaO carbonation in both the kinetic controlled and the diffusion controlled regimes. The continuous model assumes that the diffusion of gaseous reactants into the particle is rapid enough in comparison to the surface chemical reaction whereas the unreacted core model, also known as the shrinking core, assumes that the reaction zone is restricted to a thin front advancing from the outer surface into the particle (Lee, 2004). While the shrinking core model could be applied to surface reaction limited regime, since the model predicts complete conversion, it is not good for properly describing the actual kinetic behavior in the diffusion controlled regime.

Another proposed model, known as the random pore model, has also been developed to describe the CO_2 - CaO gas-solid chemical reaction kinetics by correlating the reaction behavior with internal pore structure (Bhatia and Perlmutter, 1983):

$$\frac{1}{\psi}\left[\sqrt{1-\psi\ln(1-X)}-1\right]=k't \tag{3.2}$$

$$\frac{1}{\psi}\left[\sqrt{1-\psi\ln(1-X)}-1\right]=k''\sqrt{t} \tag{3.3}$$

where ψ is a structural parameter depending on the surface area, porosity, and the initial total length of the pore system per unit volume and k', k'' are rate constants. Note that Equation 3.2 is for the chemical reaction controlled regime and Equation 3.3 for the diffusion controlled regime. Although this model is useful for understanding by what structural parameters the rate of CaO carbonation reaction is determined it is quite complex and difficult to employ in a reactor model. From a modeling perspective, it would be more practical to utilize an apparent kinetic model. By this method, experimental CaO conversion versus time data can be implemented into a best fit kinetic equation resulting in the determination of a single rate constant over both the chemical reaction and diffusion controlled regimes.

3.2.1 – Apparent Kinetic Model

From visual inspection of Figure 3.1, it can be easily inferred that the rates of carbonation are rapid at low conversion levels (surface reaction limited) and begin to decrease as the conversion approaches the ultimate conversion X_u. The ultimate conversion is defined as the point where there is no significant change in conversion (>95 %) and the rate of conversion approaches zero. Therefore, if the initial rate of CaO conversion is represented by a constant, k, then the rate of conversion can be expressed as follows (Lee, 2004):

$$\frac{dX}{dt}=k\left(1-\frac{X}{X_u}\right)^n \tag{3.4}$$

where n is a parameter. At the early stages of the CaO carbonation reaction, where the conversions are low, the $(1-(X/X_u))$ term reduces to one indicating that the rate of carbonation is dependant only on the rate constant k. Lee (2004) proposed that the value of k can be regarded as the intrinsic chemical rate constant on the CaO surface.

Although this may be true, a more accurate method for determining the intrinsic chemical rate constant would be the use of a grain model, with kinetic control, due the near spherical nature of most natural occurring calcium based calcines (Sun et al., 2008b). This type of gas-solid chemical reaction kinetics model will be discussed in detail in Section 3.2.2.

As the conversion increases, the rate of conversion decreases by the attenuation term, $(1-(X/X_u))^n$, and becomes zero at $X = X_u$. Thus, in order to determine the conversion as an explicit function of time, a value for the power n must be selected. Lee (2004) indicated that the value for n should be taken as either 1 or 2. From integration of Equation 3.4, using both values for n, results in the following equations:

$$X = X_u\left[1-\exp\left(-\frac{k}{X_u}t\right)\right] \tag{3.5}$$

$$X = \frac{X_u t}{(X_u/k)+t} \tag{3.6}$$

where Equation 3.5 and 3.6 are for $n=1$ and $n=2$ respectively. The least-square regression analysis performed by Lee (2004) of carbonation data taken from Bhatia and Perlmutter (1983) and Gupta and Fan (2002) using both Equations 3.5 and 3.6 shows that Equation 3.6 is more appropriate to correlate the carbonation data. The regression analysis, using Equation 3.6, gives a poorest correlation coefficient of 0.95 while Equation 3.5 a best correlation coefficient of 0.91 over a temperature range of 550 to 725 ^{o}C. This result has been further reinforced by carbonation data gathered by (Lee et al., 2004) over a similar temperature range. It should be noted that Equation 3.5 has been adopted for the kinetics of the reaction between CO_2 and $Ca(OH)_2$ in humid conditions at low temperatures (Shih et al., 1999). The expression was derived assuming the carbonation rate is controlled by the chemical reaction on the $Ca(OH)_2$ surface and taking into account the surface coverage by product ($CaCO_3$). Based on the carbonation data collected for this work, Equation 3.5 has been determined to more appropriately correlate the date. Although this result contradicts to the work of Lee, Equation 3.5 will be used

for the determination of the kinetic rate constant and the ultimate conversion and Equations 3.6 will not be considered further in the present study.

In order to determine the rate constants from carbonation conversion data Equation 3.5 must first be manipulated into the following form:

$$1-\frac{X}{X_u}=\exp\left(-\frac{k}{X_u}t\right) \tag{3.7}$$

Now taking the natural logarithm of each side of Equation 3.7:

$$\ln\left(1-\frac{X}{X_u}\right)=-\frac{k}{X_u}t \tag{3.8}$$

Due to the nature of Equation 3.8, the kinetic parameters k and X_u cannot be directly determined by least-square regression analysis. First a value of X_u must be assumed, then by plotting the left hand side of Equation 3.8 versus time the value of k can be determined by adjusting the value of X_u to minimize the least-square regression error. After this iterative procedure has been completed the value of k can be determined via the following formula:

$$k=-slope \tag{3.9}$$

where *slope* is the slope of the least-square regression analysis.

3.2.2 – Intrinsic Surface Reaction Kinetics / Grain Model

As mention in Section 3.2.1, a grain model (shrinking core model) is unsuitable for properly describing the actual kinetic behavior over the entire chemical reaction between CO_2 and CaO. This is true due to the diffusion controlled regime of the reaction when the surface chemical kinetics are not limiting. When determining the intrinsic surface chemical rate constant and activation energy for the gas-solid reaction, a grain model with kinetic control is appropriate for defining the kinetically controlled region

due to the near spherical nature (of the micrograins) of most calcined limestones and dolomites (Sun et al., 2008b).

Such a grain model under kinetic control for spherical micrograins is as follows (Szekely et al., 1976). It should be noted that this model assumes no external mass transfer limitations from the bulk gas to the particle surface.

$$\frac{dX}{dt(1-X)^{2/3}} = 3 \cdot r \tag{3.10}$$

where r is the reaction rate. Taking the integral of Equation (3.10) gives:

$$1-(1-X)^{1/3} = r \cdot t \tag{3.11}$$

Thus, by plotting $(1-(1-X)^{1/3})$ versus t, this should result in a straight line of slope r for the kinetically controlled regime of the gas-solid reaction. From Figure 3.2, it can be observed that at the start of the reaction there is a short induction period (approximately 20 seconds), followed by a short mass breakthrough stage with maximum slope and ending with a gradual slow down. The short mass breakthrough stage indicates the kinetically controlled region of the gas-solid reaction with the slope of this line representing the intrinsic surface reaction rate r. This region features the maximum slope obtained before the slow down stage where the reaction is controlled by both surface kinetics and product layer diffusion. It should be noted that as the reaction proceeds further, that product layer diffusion becomes a larger factor and slows down the rate of carbonation to near zero as the conversion approaches X_u.

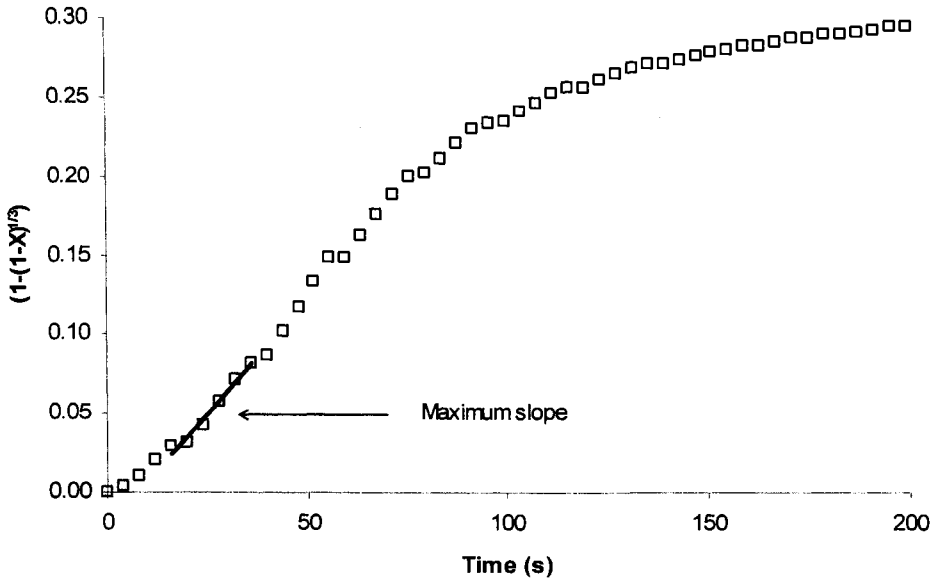

Figure 3.2: Slope extraction from grain model carbonation for 250-425 micron Havelock limestone particles at 620°C with 8% CO_2, 21% H_2, 42% CO, 17% H_2O, and 12% N_2.

Although the induction period shows a lower rate of carbonation, this stage should belong to the kinetically controlled region. Therefore, the value of the intrinsic surface reaction rate, r, can be extended to represent the true rate at the time $t = 0$ and $X = 0$ (Sun et al., 2008b) thus,

$$r = r_0 \tag{3.12}$$

where r_0 is the intrinsic surface reaction rate at time $t = 0$. For most heterogeneous gas-solid reactions the reaction rate is more conveniently expressed as a specific rate, R:

$$R = \frac{dX}{dt(1-X)} \tag{3.13}$$

When the reaction is under kinetic control, the specific rate can also be expressed in a power law form relating the change in conversion with time to the partial pressure of CO_2, P_{CO_2}, to the power of the reaction order:

$$R = 56 \cdot k_s \cdot S(P_{CO_2} - P_{CO_2,eq})^a \tag{3.14}$$

where 56 is the molecular weight of CaO, k_s is the intrinsic surface reaction rate constant, S is the specific CaO surface area, and a is the reaction order. Equation 3.10 can be rearranged in terms of a specific rate giving:

$$\frac{dX}{dt(1-X)} = 3 \cdot r(1-X)^{-1/3} \tag{3.15}$$

and equating Equations 3.14 and 3.15 leads to:

$$3 \cdot r(1-X)^{-1/3} = 56 \cdot k_s \cdot S(P_{CO_2} - P_{CO_2,eq})^a \tag{3.16}$$

Now taking the initial condition that at time $t = 0$, when the surface area is $S = S_0$ and $X = 0$, Equation 3.16 simplifies to:

$$3 \cdot r_0 = 56 \cdot k_s \cdot S_0(P_{CO_2} - P_{CO_2,eq})^a \tag{3.17}$$

To determine the intrinsic surface rate constant, k_s, from Equation 3.17, the value of the reaction order, a, must first be determined. From work performed by Bhatia and Perlmutter (1983), it was observed that the intrinsic reaction order of the carbonation reaction was first order with respect to CO_2 partial pressure in the 0 to 10 kPa range. Complementary studies carried out by Kyaw et al. (1996) showed a close to zero intrinsic reaction order for higher CO_2 partial pressures (> 10 kPa). Both of these results have been recently confirmed by Sun et al. (2008b).

Due to the scope of this thesis, CO_2 partial pressures higher than 10 kPa will not be explored thus, the value of a in every case will be one. Substituting $a = 1$ into Equation 3.17 and rearranging gives:

$$k_s = \frac{3}{56} \cdot \frac{r_0}{S_0(P_{CO_2} - P_{CO_2,eq})} \tag{3.18}$$

Therefore, the intrinsic surface rate constant can be determined at a specific temperature assuming that the specific CaO surface area in known. With the use of the Arrhenius equation and several k_s values, at varying temperatures, the activation energy of the gas-solid reaction between CO_2 and CaO can now be determined:

$$k_s = k_0 \exp\left(-\frac{E}{R_g T}\right) \tag{3.19}$$

where k_0 is the pre-exponential factor, E is the activation energy, and R_g is the gas constant. In logarithmic form, Equation 3.19 becomes:

$$\ln(k_s) = \ln(k_0) - \frac{E}{R_g T} \tag{3.20}$$

A plot of $\ln(k_s)$ versus $1/R_g T$ results in a straight line with slope equal to the activation energy, E, and a y-intercept equal to the natural logarithm of the pre-exponential factor, k_0.

3.3 – Reactor Models

Fluidized beds have been a natural choice for carbonator reactors for the capture of CO_2, both because of the high enthalpy release from the carbonation reaction and the high reaction rates required (Abanades et al., 2004). These types of beds have already been used in practice for CO_2 capture using CaO in the acceptor gasification process operating at high pressure (Curran et al., 1967). As well, Abanades et al. (2004) has shown that a fluidized bed of CaO can be a suitable reactor to achieve very effective CO_2 capture efficiencies from typically low CO_2 partial pressures of combustion flue gases. Unfortunately, long term problems have arisen with the use of CaO particles in fluidized bed reactors. Attrition of the particles results in significant losses of the sorbent and it is for this reason that a moving bed reactor has been proposed for the following reactor model (Jia et al., 2007).

Up to date there is limited or no information available on the actual performance of a moving bed of CaO working as a CO_2 capture system at low CO_2 partial pressures of gasification flue gases. Therefore, the objective of this section is to develop a suitable mathematical model for a moving bed carbonator reactor by linking kinetic data obtained via an apparent kinetic model (Section 3.2.1) with a reasonable description of the gas-solid contact.

3.3.1 – General Differential Mass Balance Equation

The following schematic, Figure 3.3, represents a typical moving bed carbonator reactor. The gaseous reactant, in this case CO_2, is feed through a moving bed where it comes into contact with CaO and reacts to form $CaCO_3$. Assuming constant reactor diameter, axial plug flow, flat radial concentration profile, constant bed void fraction and uniform particle size, the general pseudo-homogeneous model (Feyo De Azevedo et al., 1990) of the differential mass balance can be written as follows:

$$\varepsilon \frac{dF_{CO_2}}{dt} = -\frac{d\left(u_g F_{CO_2}\right)}{dz} - \nu(1-\varepsilon)\rho_{CaO} r_{cbn} \tag{3.21}$$

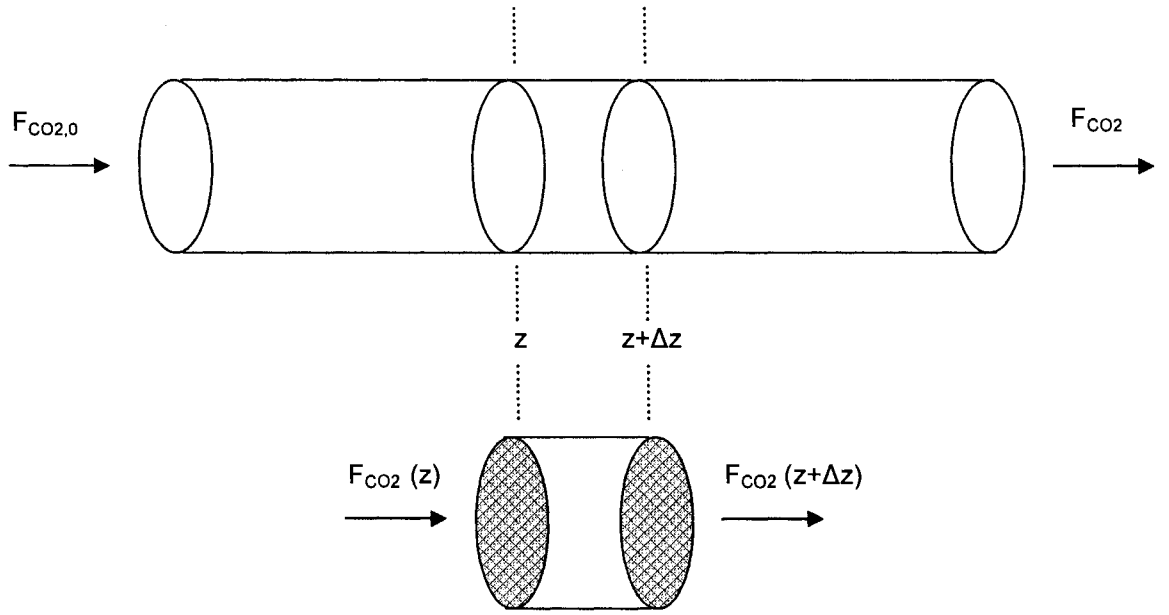

Figure 3.3: Fixed / moving bed reactor schematic.

where F_{CO_2} is the molar flowrate of CO_2, z is the axial distance from the inlet of the reactor, t is the time the CaO bed has been exposed to CO_2, u_g is the superficial velocity of the bulk gas through the bed, ε is the bed void fraction, ρ_{CaO} is the apparent density of the CaO particles, ν is the volumetric flow rate of the bulk gas, and r_{cbn} is molar rate of CO_2 removal per unit mass of CaO. Equation 3.21 can also be expressed in terms of CO_2 molar concentration, C_{CO_2}, by the following relationship:

$$C_{CO_2} = \frac{F_{CO_2}}{\nu} \tag{3.22}$$

Thus, Equation 3.21 becomes:

$$\varepsilon \frac{dC_{CO_2}}{dt} = -\frac{d\left(u_g C_{CO_2}\right)}{dz} - (1-\varepsilon)\rho_{CaO} r_{cbn} \tag{3.23}$$

The last term on the right-hand side of Equation 3.23 represents the molar rate of CO_2 removal by CaO carbonation per unit bed-volume of the reactor. The molar rate of CO_2 removal per unit mass of CaO can be represented as:

$$r_{cbn} = \frac{\gamma}{M_{CaO}}\left(1 - \frac{X}{X_u}\right) \tag{3.24}$$

where M_{CaO} is the molecular weight of CaO and γ is a parameter introduced to account for that the local rate of CaO carbonation along the bed may be governed by kinetic limitation or by mass transfer limitation of the reactant CO_2. For the former, the rate of CaO carbonation at a given bed temperature is determined by k via Equations 3.8 and 3.9 (Section 3.2.1). For the latter case, it is determined by the availability of CO_2, which depends on the amount entrained with upcoming convective flow. Therefore, under kinetic limitation:

$$\gamma = k \tag{3.25}$$

and under mass transfer limitation:

$$\gamma = \frac{M_{CaO}}{(1-\varepsilon)\rho_{CaO}} \cdot \psi_{CO_2} \tag{3.26}$$

For a local bed zone where the CaO carbonation is under mass transfer limitation, the quantity of CO_2 removable by the carbonation of CaO corresponds to the amount of CO_2 available within the zone minus that of CO_2 escaping from the zone with a convective flow in the equilibrium CO_2 concentration, $C_{CO_2,eq}$. In Equation 3.26, ψ_{CO_2} is introduced to take into account part of the convective delivered CO_2, which is supposed to be removed by carbonation of CaO within a bed zone of a finite bed length, Δz:

$$\psi_{CO_2} = \frac{u_g\left(C_{CO_2} - C_{CO_2,eq}\right)}{\Delta z} \tag{3.27}$$

It should be noted that Equation 3.23 can be applied to both a fixed and moving bed carbonator operating at non-isothermal, non-adiabatic, and non-isobaric conditions.

3.3.2 – Moving Bed Model

For a moving bed carbonator, the general pseudo-homogeneous model of the differential mass balance of CO_2, Equation 3.23, can be applied directly with a few modifications provided the assumptions are valid. In the case of a moving bed, the reactor operates under steady-state where the solid particles are assumed to move steadily in a close-packed state along the reactor co-current with the passing flow of gas species. Thus, Equation 3.23 can be adapted into the following form:

$$\frac{d\left(u_g C_{CO_2}\right)}{dz} = -(1-\varepsilon)\rho_{CaO} r_{cbn} \tag{3.28}$$

Since the concentration of CO_2 decreases along the length of the reactor due to carbonation, the superficial velocity, u_g, will change as a function of the concentration of CO_2. As well, since the carbonation reaction is exothermic and there is a pressure drop over the bed length the superficial velocity must be corrected to account for these variables as follows:

$$u_g = u_{g,0}\left(\frac{\left(C_T - C_{CO_2,0}\right) + C_{CO_2}}{C_T}\right)\cdot\frac{P_0}{P}\cdot\frac{T}{T_0} \tag{3.29}$$

where $u_{g,0}$ is the inlet superficial velocity of the bulk gas through the bed, $C_{CO_2,0}$ is the inlet molar concentration of CO_2, C_T is the total inlet molar gas concentration, P is the system pressure, P_0 is the inlet pressure, T is the system temperature, and T_0 is the inlet

gas temperature. To obtain the axial profile of the fractional conversion, X, of the moving solid CaO by carbonation, the mass balance is given by:

$$\frac{dX}{dz} = \frac{M_{CaO}}{u_s} r_{cbn} \tag{3.30}$$

where u_s is the linear velocity of the solid particles along the reactor. It is assumed the linear velocity, u_s, does not vary with changes in temperature or pressure. The pressure distribution in the moving bed reactor is assumed to follow the Ergun equation (Ergun, 1952) for a fixed bed reactor and cab expressed as follows:

$$\frac{dP}{dz} = -\frac{\rho_g u_g^2}{d_p} \cdot \frac{1-\varepsilon}{\varepsilon} \left(\frac{150(1-\varepsilon)\mu}{d_p \rho_g u_g} + 1.75 \right) \tag{3.31}$$

where ρ_g is the density of the bulk gas, d_p is the CaO particle diameter (assumed constant), and μ is the gas phase viscosity. It should be noted that the gas phase density, ρ_g, and viscosity, μ are assumed to remain constant over the temperature and pressure range explored in this study. The steady-state pseudo-homogeneous energy balance for the moving bed reactor can be written as:

$$\left[\rho_g u_g C_{pg} + (1-\varepsilon)\rho_{CaO} C_{ps}\right] \frac{dT}{dz} = -(1-\varepsilon)\rho_{CaO} r_{cbn} H_{cbn} + h_w (T_w - T) \frac{4}{d_r} \tag{3.32}$$

where C_{pg} and C_{ps} are the gas and solid heat capacities respectively, H_{cbn} is the heat of CaO carbonation reaction, h_w is the wall-bed heat transfer coefficient, T_w is the reactor wall temperature, and d_r is the inner diameter of the reactor. As was the case with the gas phase density, ρ_g, it has been assumed that the gas heat capacity, C_{pg}, and the heat of CaO carbonation reaction, H_{cbn}, remain constant over the temperature and pressure range explored in this study. Since the heat capacity of CaO varies greatly with

temperature the following equation is used to determine the heat capacity over the temperature range used in this work.

$$C_{ps} = 10.00 + 0.00484T - 108000/T^2 \tag{3.33}$$

The wall-bed heat transfer coefficient, h_w, can be determined by the following correlation proposed by Li and Finlayson (1977) for a packed tube reactor at low feed flow rates.

$$h_w = 2.03\left(\frac{k_g}{d_r}\right)\mathrm{Re}_p^{0.8}\exp\left(-\frac{6d_p}{d_r}\right) \tag{3.34}$$

for $\mathrm{Re}_p = 20 - 7600$ and $d_p/d_r = 0.05 - 0.3$

where k_g is the thermal conductivity of the bulk gas and Re_p is the particle Reynolds number defined as follows:

$$\mathrm{Re}_p = \frac{u_g \varepsilon \rho_g d_p}{\mu} \tag{3.35}$$

3.3.3 – Numerical Method

The model equations described above are considered as initial value problems of ordinary differential equations with given conditions at the reactor entrance with respect to the concentration of the feed gas (Equation 3.28), total pressure (Equation 3.31), and temperature (Equation 3.32). Starting with the inlet conditions, the differential equations are solved by successive integration of all the spatial sections along the reactor. These operations are performed via the use of MATLAB version 7.1, where the set of ordinary differential equations, along with the initial conditions, are discretized in the z-direction using forward finite differences. For finite differences, the reactor of bed length $L = 0.50$

m was divided into 100 sections with 101 nodes. A summary of the parameter values used in the simulation are listed in Table 3.3.

Table 3.3: Values for parameters used in moving bed reactor simulation.

Parameters	Values	Units
C_{pg}	1.650	kJ/(kg.K)
d_r	0.1	m
d_p	4.25E-04	m
H_{cbn}	-1.788E+05	kJ/kmol
k_g	1.01E-04	kJ/(m.s.K)
M_{CaO}	56	kg/kmol
ε	0.75	-
μ	3.32E-05	Pa.s
ρ_{CaO}	1620	kg/m^3
ρ_g	0.2909	kg/m^3

Chapter 4 – Results and Discussions

The following chapter presents the experimental results and discussion regarding the effect of carbonation / calcination conditions on the carbonation reaction kinetics along with sorbent deactivation for a naturally occurring limestone and dolomite. As well, a sensitivity / parametric analysis has been performed on a moving bed carbonator reactor model developed in Chapter 3 and will be evaluated in detail in this chapter.

4.1 – Naturally Occurring Limestone – Havelock

4.1.1 – Effect of Carbonation Feed Gas

Table 4.1 lists the intrinsic rate constants of the CaO-CO_2 reaction at 620°C for 250-425 micron Havelock limestone particles under two different carbonation feed gas compositions. It can be seen that the rate of carbonation is roughly 70 % greater when the Havelock particles are carbonated with CO and H_2 in the feed gas. As indicated in Chapter 3.2.2, for CO_2 partial pressures less than 10 kPa, the carbonation reaction rate is

Table 4.1: Intrinsic rate constants for 250-425 micron Havelock limestone particles carbonated at 620°C for two different carbonation feed gas compositions.

Feed Gas Composition (vol%)	Total Pressure (atm)	Carbonation Temperature (°C)	r_0 (1/s)	k_s (mol/m^2.s.kPa)
8 CO_2, 21 H_2, 42 CO, 17 H_2O, 12 N_2	1	620	0.0029	1.29E-06
8 CO_2, 17 H_2O, 75 N_2	1	620	0.0017	7.58E-07

solely a function of the particle surface area, carbonation temperature, and CO_2 partial pressure. Since the experiments were performed using "nominally" identical limestone samples and reaction temperatures, this might indicate that difference in the rates of reaction is related to the CO_2 partial pressure. However, as the partial pressure of CO_2 is 0.08 atm for both carbonation feed gases, thus, the difference in reaction rate must be associated with partial pressure of CO_2 at the CaO surface.

Experiments performed by Han and Harrison (1994) on the simultaneous shift reaction and carbon dioxide separation for the direct production of hydrogen has shown that the water-gas shift reaction proceeds in the absence of a heterogeneous shift catalyst

at temperatures in the vicinity of 550°C. A number of metals and metal oxides are known shift catalysts (Rofer-DePoorter, 1984) but no references to CaO catalyzing the reaction, other than the above, have been located. Although not measured during the TGA experiments, based on the work of Han and Harrison, it becomes plausible that the water-gas shift reaction indeed takes place and is catalyzed on the surface of the Havelock limestone particles.

Due to the shift in apparent reaction order, as described in Chapter 3.2.2, it follows that the CaO-CO_2 reaction might follow a series of elementary steps (Sun et al., 2008b). The following is a two step Langmuir mechanism with $CaO{\cdot}CO_2$ as the intermediate complex:

$$CaO + CO_2 \leftrightarrow CaO{\cdot}CO_2 \tag{4.1}$$

$$CaO{\cdot}CO_2 \leftrightarrow CaCO_3 \tag{4.2}$$

Step 1 involves a reversible process with gaseous CO_2 molecules adsorbing on the CaO sites to give $CaO{\cdot}CO_2$ intermediate complexes. Step 2 involves reaction to produce solid product. It is now assumed that step 1 is rate controlling when the driving force is less than 10 kPa, as is the case of the above experimental conditions (Sun et al., 2008b). Therefore, the CO_2 concentration at the CaO surface will essentially determine the rate of the CaO-CO_2 reaction. Returning to the hypothesis that the water-gas shift reaction is taking place and is catalyzed on the surface of the limestone particles, it is reasonable that the local concentration of CO_2 at the particle surface would be higher with the addition of CO and H_2 with an identical CO_2 partial pressure in the bulk gas. This phenomenon can be further supported by examination of Figure 4.1.

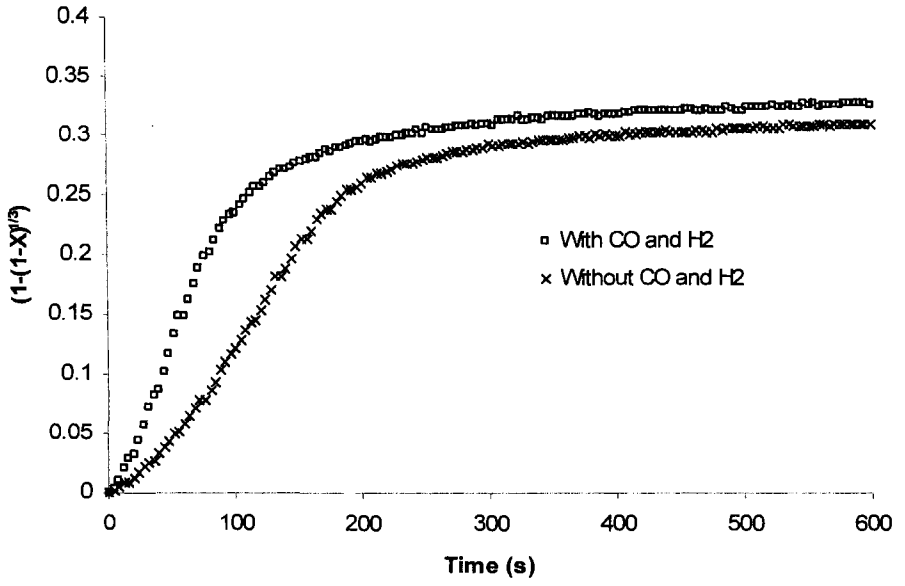

Figure 4.1: Grain model plot for 250-425 micron Havelock limestone particles calcined at 850°C with N_2 and carbonated at 620°C with and without CO and H_2.

Listed in Table 4.1 are the initial rates of carbonation before the slow-down stage which is controlled by both surface reaction and product-layer diffusion. Figure 4.1 shows a plot of the grain model versus time described in Chapter 3.2.2 where the slope at any given time is equal to the rate of carbonation. Here the slow-down stage can be observed for both carbonation feed gas conditions but it should be pointed out that this stage occurs approximately 100 seconds earlier in the case where CO and H_2 are presence in the feed gas. This would indicate that the rate of carbonation is greater under these conditions even as the reaction proceeds partially limited by product-layer diffusion. This could be explained via the water-gas shift argument since, in the case where CO and H_2 are not present; the rate of carbonation is partially limited by the diffusion of CO_2 through the $CaCO_3$ product layer resulting in a CO_2 surface concentration lower than that of the bulk gas. Conversely, when CO and H_2 are present in the bulk gas they may diffuse through the $CaCO_3$ product layer and react on the CaO surface producing CO_2 and consequently increase the CO_2 surface concentration to a level higher than without CO and H_2 present in the feed gas.

This phenomenon becomes significant as the CaO-CO_2 reaction proceeds and is increasingly limited by the product-layer diffusion. Looking at Figure 4.1, once the reaction reaches approximately 80% of its ultimate conversion, the rate of carbonation for

both feed gases are effectively identical. This can once again be explained by the assumption that the water-gas shift reaction is catalyzed on the active CaO sites. When the reaction nears completion the number of active CaO sites is limited thus the added CO_2 surface concentration from the water-gas shift reaction is negligible in comparison to the CO_2 that has diffused through the product layer from the bulk gas. Thus, the carbonation reaction proceeds at an equivalent rate to that of the reaction where neither CO nor H_2 are present in the feed gas mixture.

As described in Chapter 2.3.2, naturally occurring limestones such as Havelock undergo deactivation over repeated cycles. The observed conversion limits are interpreted in terms of a certain loss in the porosity associated with small pores and a certain increase in the porosity associated with large pores. Thus, it is of particular interest to examine if the limited conversion is affected by carbonation feed gas composition. Using Equation 2.5 the limited conversion versus cycle number data has been fitted to determine the values of f_m and f_w for the Havelock limestone particles carbonated with and without CO and H_2 over 10 cycles.

Table 4.2: Equation 2.5 fitted parameters over 10 cycles for 250-425 micron Havelock particles carbonated at 620°C for two different carbonation feed gas compositions.

Feed Gas Composition (vol%)	Total Pressure (atm)	Carbonation Temperature (°C)	N Cylces	f_m	f_w
8 CO_2, 21 H_2, 42 CO, 17 H_2O, 12 N_2	1	620	10	0.749	0.328
8 CO_2, 17 H_2O, 75 N_2	1	620	10	0.749	0.324

From Table 4.2, it can be observed that the values of f_m and f_w for both carbonation feed gas compositions are, for all practical matters, identical. Thus, it can be concluded that the presence of CO and H_2 during the carbonation of Havelock particles has no or very little impact on the CaO conversion over 10 cycles. It should be noted that the decrease in carbonation capacity during the cycling of calcination / carbonation reactions has been attributed to sintering and pore closure (Abanades and Alvarez, 2003). It is well known that sintering during calcination is favoured both by high temperatures and time at temperature (Borgwardt, 1989), and is accelerated by the presence of CO_2 and H_2O (Borgwardt, 1989). Since both samples were calcined under identical conditions

(i.e., same temperature, same time at temperature, and under pure N_2), it is reasonable that the levels of particle sintering should be similar resulting in near equal limited conversions over repeated cycling assuming that the presence of CO and H_2 during carbonation has no effect. This conclusion can be further supported by examination of Figures 4.2 – 4.5. Figures 4.2 – 4.5 are SEM images at two different magnifications (100 and 10 micron scales) for Havelock particles after 10 calcination / carbonation cycles carbonated with and without CO and H_2. Figures 4.2 and 4.3 show similar surface textures and particle shapes whereas from Figures 4.4 and 4.5 it is clear that both samples show similar formations of $CaCO_3$ product and levels of sintering as is depicted by the size of the micrograins. In both Figures 4.4 and 4.5, the average size of a micrograin is approximately 1 micron in diameter.

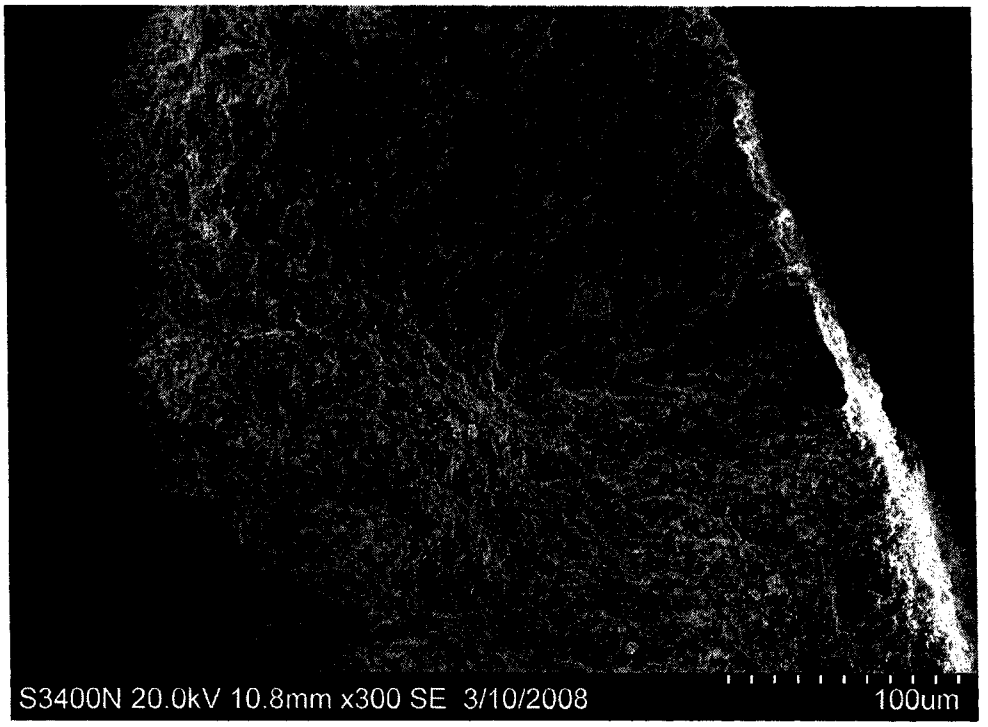

Figure 4.2: SEM image of a Havelock limestone particle after 10 calcination / carbonation cycles calcined at 850°C with N_2 and carbonated at 580°C with 8% CO_2, 17% H_2O, and 75% N_2 – 100 micron scale.

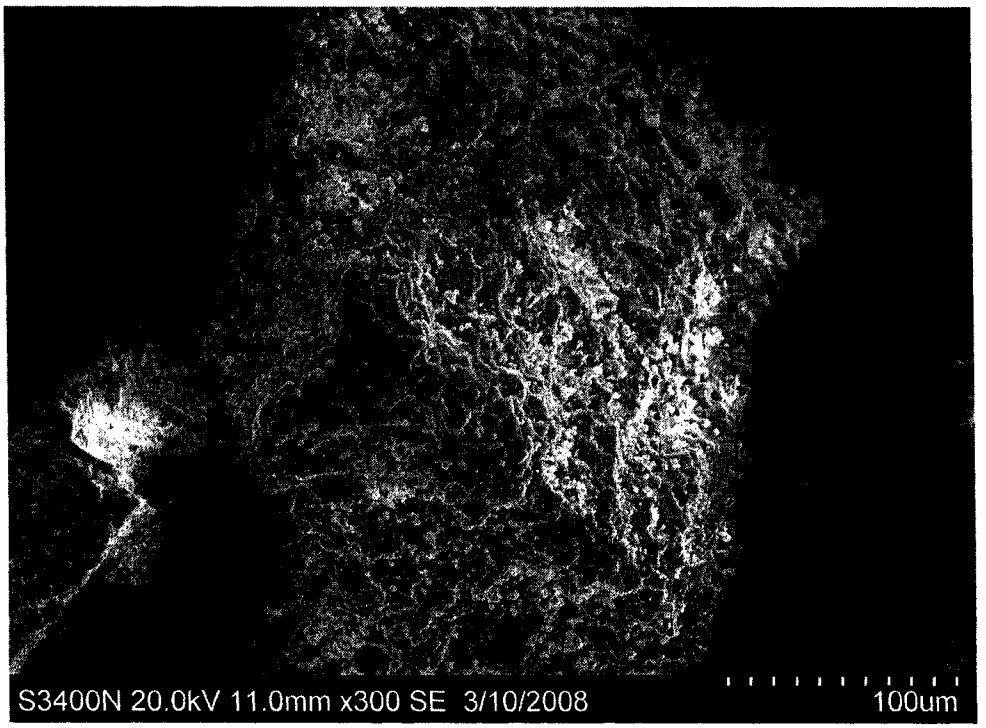

Figure 4.3: SEM image of a Havelock limestone particle after 10 calcination / carbonation cycles calcined at 850°C with N_2 and carbonated at 580°C with 8% CO_2, 21% H_2, 42% CO, 17% H_2O, and 12% N_2 – 100 micron scale.

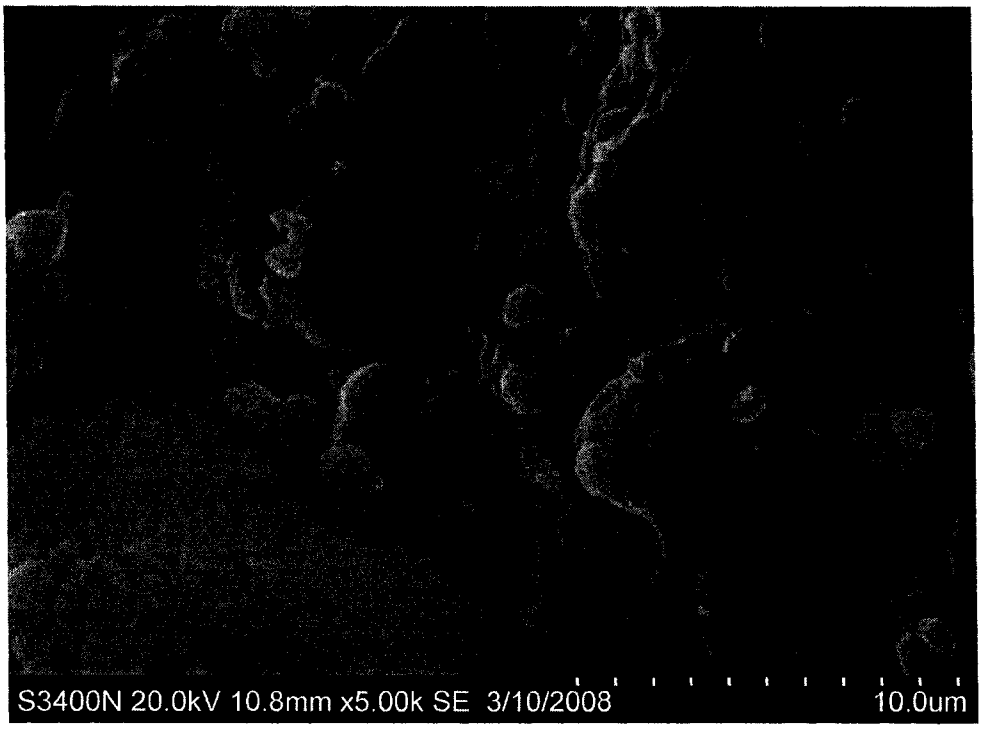

Figure 4.4: SEM image of a Havelock limestone particle after 10 calcination / carbonation cycles calcined at 850°C with N_2 and carbonated at 580°C with 8% CO_2, 17% H_2O, and 75% N_2 – 10 micron scale.

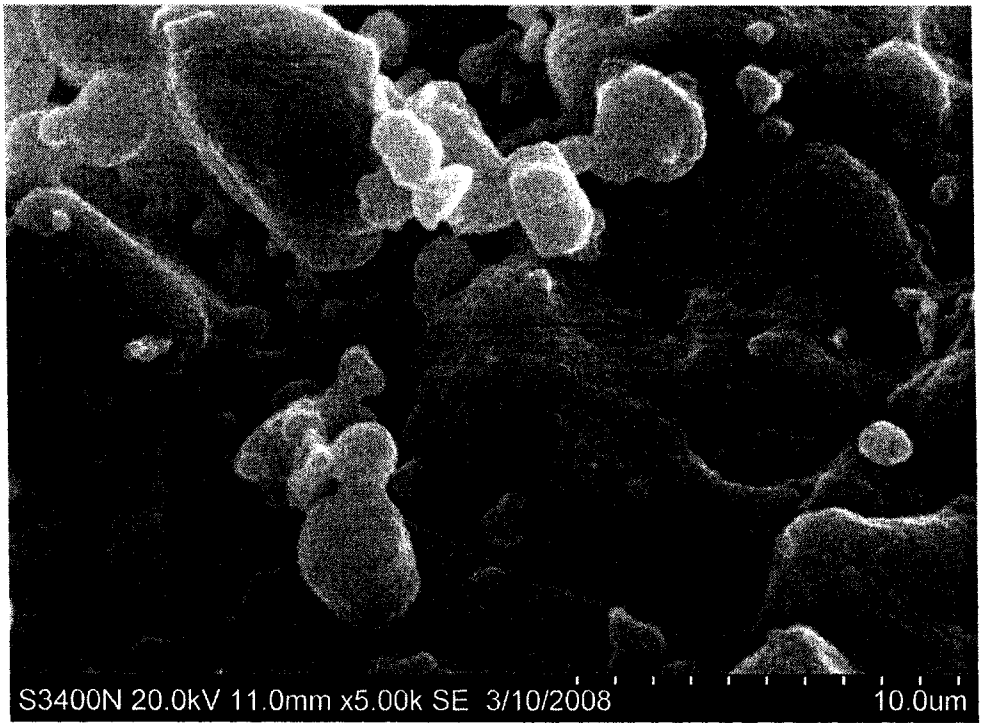

Figure 4.5: SEM image of a Havelock limestone particle after 10 calcination / carbonation cycles calcined at 850°C with N_2 and carbonated at 580°C with 8% CO_2, 21% H_2, 42% CO, 17% H_2O, and 12% N_2 – 10 micron scale.

It has been shown that the presence of CO and H_2 in the carbonation feed gas has essentially no effect on the limited carbonation over 10 cycles. It should be noted that both carbonation feed gases contain steam and should be compared to experimental runs where the feed gas contains only CO_2 and an inert (N_2 or He) in order to determine if the presence of steam has an effect on the carbonation conversion. Figure 4.6 shows the decay in maximum conversion plotted with Equation 2.5 using the fitted parameters f_m and f_w listed above in Table 4.2 for the carbonation of Havelock particles with and without CO and H_2 along with two other plots. The first, TG850/0 (Abanadas and Alvarez, 2003), was performed under similar carbonation / calcination conditions with the absence of steam, CO, and H_2 in the carbonation feed gas and the second, "Best Fit", a compilation of conversion data from experiments with varying carbonation / calcination conditions, particles sizes, and sorbent characteristics.

Looking at Figure 4.6 and comparing the decay in conversion of run TG850/0 with that of the runs containing steam it is apparent the performance of the limestone is far worse with the absence of steam during carbonation. After the tenth cycle the

carbonation conversion is approximately 30% lower. In order to understand the decrease in conversion it is useful to compare the values of f_m and f_w for each run. Since the values of f_m and f_w for the runs with and without CO and H_2 are nearly identical the following comparisons will only be made using f_m and f_w values for the run without the presence of CO and H_2. The values of f_m and f_w for run TG850/0 are 0.674 and 0.233 respectively. Comparing these values to those found in Table 4.2, both f_m and f_w are greater with the presence of steam in the carbonation feed gas. As mentioned in Chapter 2.3.2, the value of f_m is the fractional loss in sorbent microporosity (or conversion associated with this microporosity) per cycle and f_w is proportional to the product of several factors including the fractional shrinking in sorbent microporosity per cycle, the fraction of the specific surface associated with the void volumes forming the mesoporosity, and the thickness of the product layer. Thus, it becomes plausible to assume that the presence of steam during carbonation hinders the loss in microporosity per cycle and increases the formation of mesoporosity occurring in the form of larger voids/pores within the grains.

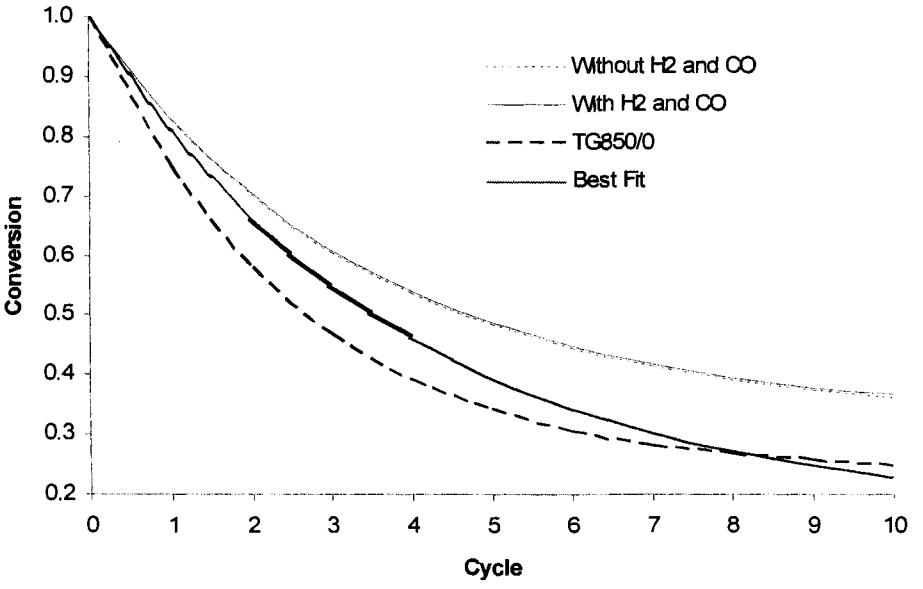

Figure 4.6: The decay in maximum carbonation conversion with the number of cycles using Equation 2.5 for 250-425 micron Havelock limestone particles calcined at 850°C with N_2 and carbonated at 620°C with and without CO and H_2 along with work performed by Abanadas and Alvarez (2003)(Without H_2 and CO $R^2 = 0.9757$ and with H_2 and CO $R^2 = 0.9885$).

It should be noted that there is a Japanese process known as the HyPr-Ring (Hydrogen Production by reaction Integrated Gasification) where coal is steam gasified, and $Ca(OH)_2$ is used to absorb CO_2, which is then regenerated (Lin et al., 2005). In order for the gasification reaction to occur at a high enough rate, and for the formation of $Ca(OH)_2$ to be possible, temperatures are of the order of 650°C, with a corresponding pressure of 3 MPa. It has been shown that the use of $Ca(OH)_2$ to capture CO_2 was significantly less susceptible to pore pluggage due to the pores lying predominately in the mesoporous range (Gupta and Fan, 2002). The precipitated CaO was also capable of maintaining its high reactivity (>90% conversion) over two calcination / carbonation cycles. Unfortunately, neither of these processes lie within the carbonation conditions explored here, and both have potential problems. The HyPr-Ring process operates at elevated pressures, while the work of Gupta and Fan involves precipitation of CaO at atmospheric conditions but with temperatures well below 600°C (typically between 90-110°C). Thus, it is impossible to draw conclusions on the effect of steam during carbonation based on these studies. However, it is interesting to note that in a recent study on the carbonation of fly ash in oxy-fuel CFB (circulating fluidized bed) combustion conditions evidence was advanced for the transient formation of $Ca(OH)_2$ during carbonation with steam, resulting in a increased carbonation conversion (Wang et al., 2008).

In order to support the argument that the carbonation of CaO with steam present, results in a smaller decrease in microporosity per cycle and increases the formation of mesoporosity occurring in the form of larger voids/pores within the grains, it is of interest to compare surface morphologies with and without steam present during carbonation. Figure 4.7 and 4.8 illustrate the differences in surface morphologies of limestone particles carbonated with and without steam respectively. Although no conclusions can be drawn about the variations in microporosity it is evident that the addition of steam results in the creation of many larger voids which can be associated with an increase in macroporosity. As the number of cycles increase, the microporosity decreases and eventually is completely eliminated resulting in only the larger voids available for carbonation. Thus, it is reasonable to assume that an increase in the number of large voids will result in a higher CaO conversion over repeated cycles as is the case here.

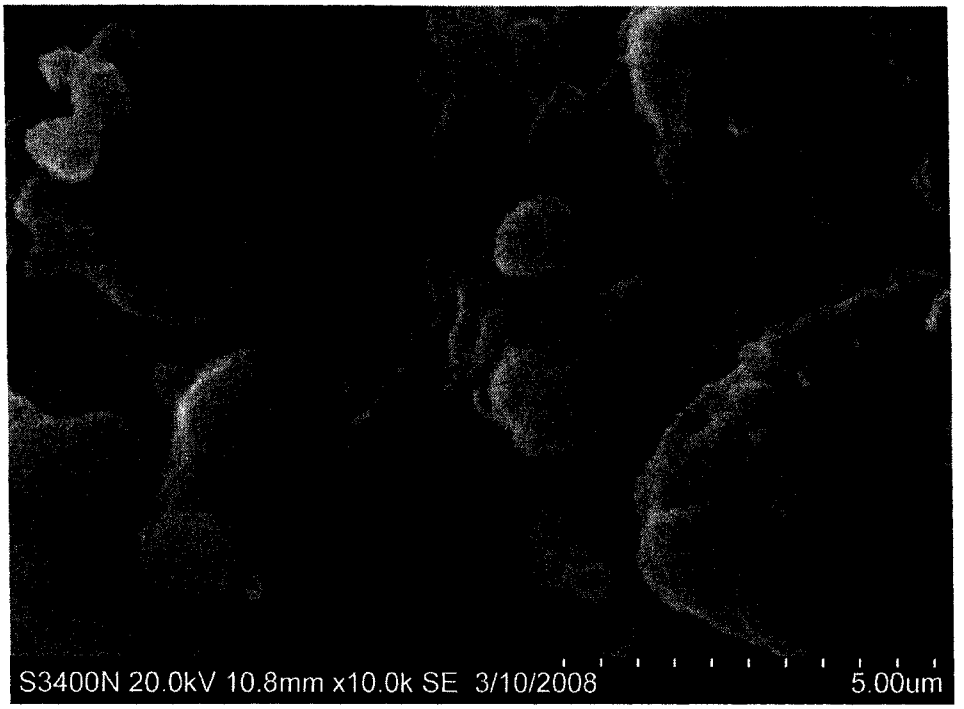

Figure 4.7: SEM image of a Havelock limestone particle after 10 calcination / carbonation cycles calcined at 850°C with N_2 and carbonated at 580°C with 8% CO_2, 17% H_2O, and 75% N_2 – 5 micron scale.

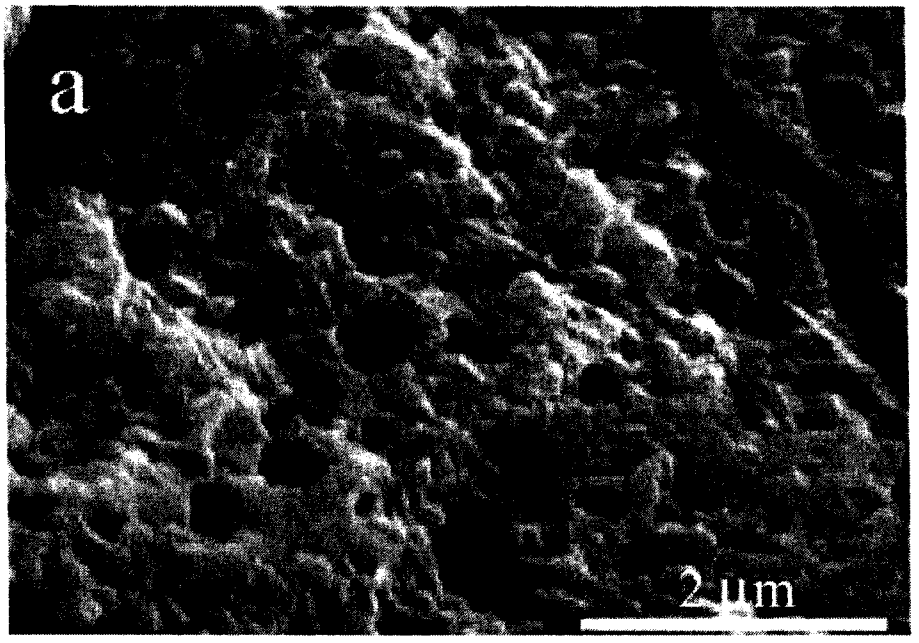

Figure 4.8: SEM image of a "la Blanca"/Omyacarb limestone particle after 7 calcination / carbonation cycles calcined at 850°C with N_2 and carbonated at 650°C with 10% CO_2 and 90% N_2 – 2 micron scale (Abanadas and Alvarez , 2003).

A similar trend can be observed in Figure 4.6 for the "Best Fit" conversion data. In this case, experiments with varying carbonation / calcination conditions, particles sizes, and sorbent characteristics have been compiled and averaged to give a reasonable mathematical description for the decay in CaO conversion with increasing cycle number. The value of f_w for the "Best Fit" data is 0.17 indicating that an increase / decrease in CO_2 partial pressure in the carbonation feed gas, the presence of CO_2 during calcination and the particle size do not result in higher CaO conversion associated with the larger voids. This confirms the assumption that the presence of steam is a major contributor for the increase in CaO conversion over repeated cycles.

4.1.2 – Effect of Carbonation Temperature

In order to quantify the reaction kinetics and obtain the activation energy for the CaO-CO_2 reaction it is necessary to carbonate at several different temperatures. As outlined in Chapter 3.2.2, the intrinsic rate constant can be determined for each temperature and via the use of the Arrhenius equation the activation energy for the carbonation reaction can be determined. Figure 4.9 shows such a plot for Havelock limestone particles carbonated with the addition of CO and H_2.

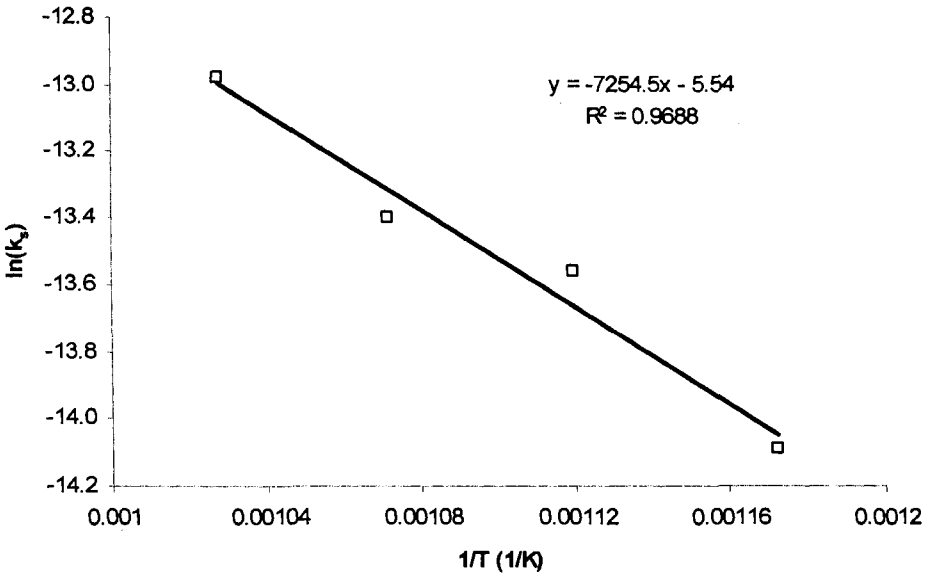

Figure 4.9: Arrhenius plot for 250-425 micron Havelock limestone particles calcined at 850°C with N_2 and carbonated with 8% CO_2, 21% H_2, 42% CO, 17% H_2O, and 12% N_2.

As expected, the intrinsic rate constants increased with increasing temperature, and the calculated activation energy is 60.3 kJ/mol. By comparison, this value is approximately double that of carbonation in the absence of CO and H_2 during carbonation (29.7 kJ/mol) as can be seen in Figure 4.10. As discussed in Chapter 4.1.1, it has been shown that the enhancement in the rate of carbonation is potentially due to the catalyzed water-gas shift reaction on the active CaO surface sites. Thus, a plausible explanation for this increase in activation energy might be that the CO_2 molecules are reacting with CaO molecules that form intermediate complexes with CO and H_2O via the water-gas shift reaction. The intermediate bonds of CO and H_2O on the CaO surface sites could increase the energy required for carbonation as the complexes increase the number of bonds per ion needed to be broken which can be directly associated with the activation energy. It should be noted that activation energy determined in the absence of CO and H_2 compares well with the value determined by Sun et al. (2008b) which was 29 ± 4 kJ/mol for 38-45 micron Strassburg limestone particles. This value was determined by a similar method described in Chapter 3.2.2. Although these values are similar, they differ greatly from the results of Bhatia and Perlmutter who, based on specific rate law analysis, reported that the CaO-CO_2 reaction has a zero-activation energy in the kinetic-controlled region. This work was supported by Dennis and Hayhurst (1987) based on equilibrium analyses and calcination data. On the other hand, these values are lower than values reported by Kyaw et al. (1996) who found an activation of 78 kJ/mol for limestone.

It is also of great importance to determine if an increase or decrease in temperature has an impact on the limited CaO conversion over repeated calcination / carbonation cycles. Figure 4.11 shows the decay in CaO conversion over 10 calcination / carbonation cycles for 4 temperatures ranging from 580 to 700°C with the presence of CO and H_2 during carbonation. From Figure 4.11, the carbonation temperature has little or no effect on the maximum carbonation conversion over repeated cycles. This result is not in agreement with experiments performed by Sun et al. (2008a), Bhatia and Perlmutter (1983), and Gupta and Fan (2002) whose work showed an increase maximum conversion with increased temperature. Over a temperature range of 500 to 850°C the CaO conversion varied between 0.4 and 0.9 for a 20 minute carbonation period as is the case for all carbonation runs in this work. It should be mentioned that although the

partial pressure of CO_2 in the carbonation feed gas varies in the various studies discussed here, it has been confirmed by the work of Sun et al. (2008a) that carbonation is insensitive to the CO_2 partial pressure in terms of the final conversion.

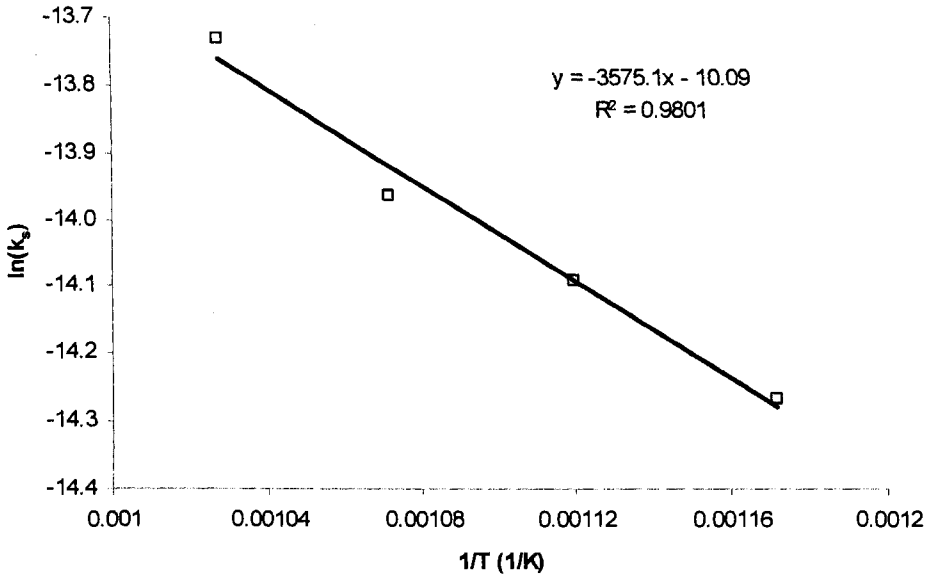

Figure 4.10: Arrhenius plot for 250-425 micron Havelock limestone particles calcined at 850°C with N_2 and carbonated with 8% CO_2, 17% H_2O, and 75% N_2.

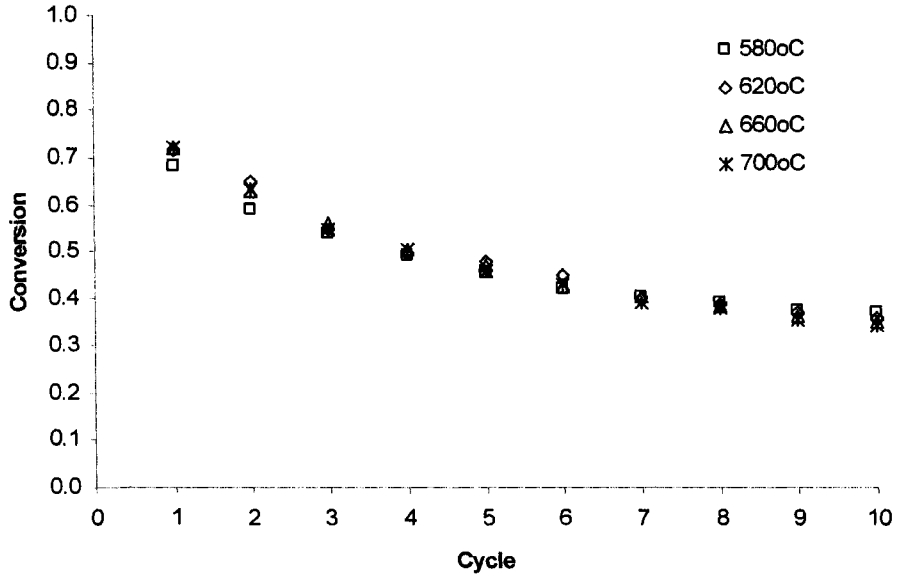

Figure 4.11: The decay in maximum carbonation conversion with the number of cycles for 250-425 micron Havelock limestone particles calcined at 850°C with N_2 and carbonated at 4 temperatures with 8% CO_2, 21% H_2, 42% CO, 17% H_2O, and 12% N_2.

It is unclear at the moment as to why some authors observe an increase in CaO conversion with increasing temperature. Based on identical calcination conditions, which dictates the level of particle sintering and change in particle porosity, it seems reasonable, that, provided a sufficient duration for carbonation, the maximum carbonation conversions should be nearly identical for all carbonation temperatures. It should be noted that some variability in maximum conversion, as seen in Figure 4.11, is expected as the limestone samples are relatively small which can lead to a variance in CaO content and average particle size from sample to sample. Based on BET N_2 adsorption analysis, the Havelock particle surface area changes from approximately 16.00 to 19.95 m^2/g when the particle size range is decrease from 250-425 to 45-150 micron, respectively. As well, there is a shift in the proportion of particle porosity from nearly all in the micropores for 250-425 micron particles to a significant quantity in the macropores for 45-150 micron particles.

Comparing Figure 4.11 to Figure 4.12, there is a considerable increase in the cyclic maximum carbonation conversion variability with an average increase in conversion of approximately 0.05 from carbonation at 580 to 700°C over 10 cycles. A plausible explanation for this phenomenon is that the addition of CO and H_2, causing the water-gas shift reaction to take place on the nascent CaO sites, allows for the maximum cyclic conversion of the CaO particles within a 20 minute carbonation period. Without CO and H_2 present, the rate of carbonation is considerably decreased thus, not allowing for the attainment of full carbonation conversion within the 20 minute carbonation period. Once again, some variability can be associated to the relatively small sample size, as discussed above.

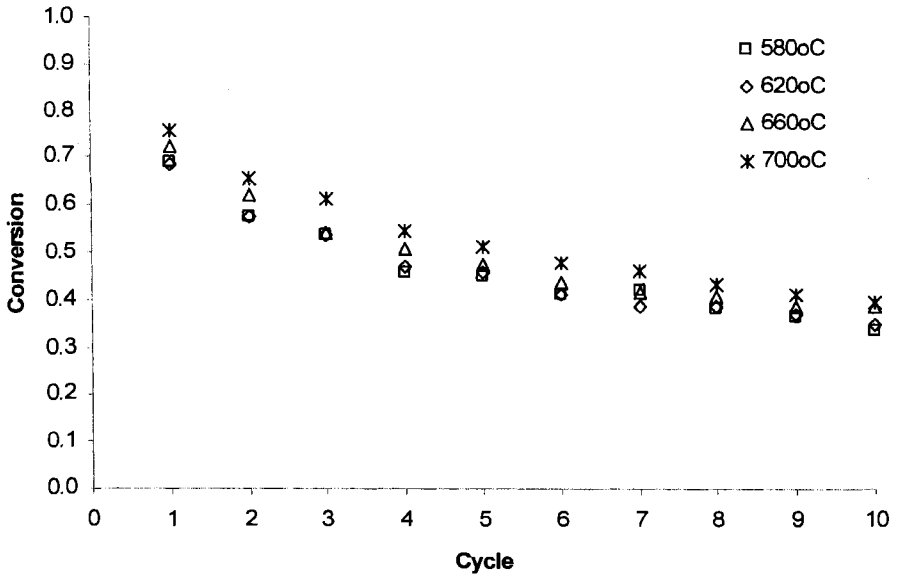

Figure 4.12: The decay in maximum carbonation conversion with the number of cycles for 250-425 micron Havelock limestone particles calcined at 850°C with N_2 and carbonated at 4 temperatures with 8% CO_2, 17% H_2O, and 75% N_2.

4.1.3 – Effect of Calcination Feed Gas

As mentioned in Chapter 4.1.1, the addition of gases such as CO_2 and H_2O during calcination have adverse effect on CaO conversion due to accelerated particle sintering and pore closure. However, there is little information on the effect of CO_2 during calcination on the initial rate of carbonation. Therefore, it is of particular interest to compare carbonation kinetics and CaO conversion, under varying calcination feed gas conditions. Table 4.3 lists the initial rates and rate constants of the CaO-CO_2 reaction at 620°C for 250-425 micron Havelock limestone particles calcined under differing feed gas conditions.

Table 4.3: Initial rates and rate constants for 250-425 micron Havelock limestone particles carbonated at 620°C with 8% CO_2, 21% H_2, 42% CO, 17% H_2O, and 12% N_2 for two different calcination feed gas compositions.

Feed Gas Composition (vol%)	Total Pressure (atm)	Calcination Temperature (°C)	r_0 (1/s)	k_s (mol/m^2.s.kPa)
90 CO_2, 10 N_2	1	915	0.0011	4.91E-07
100 N_2	1	915	0.0050	2.23E-06

From Table 4.3 it is apparent that the addition of CO_2 during calcination has a dramatic effect on the initial rate of carbonation. Under a 90% percent atmosphere of CO_2, the initial rate of carbonation is approximately 4.5 times less than with pure N_2. It is known that during sintering, necks develop between adjacent grains and continue to grow. The material for this is supplied from the rest of the grain, so that the distance between grain centers is diminished. This causes both the voidage and the surface area to decrease (Stanmore and Gilot, 2005). This decrease in voidage could explain the significant decrease in rate of carbonation as the reaction becomes limited by mass diffusion of CO_2 to the nascent CaO sites. As well, a decrease in surface area associated with the particle microporosity, where the reaction is know to proceed rapidly, would leave only larger pores for carbonation which are subject to product layer diffusion limitations. Figures 4.13 and 4.14 show the significant increase in particle grain neck growth under CO_2 calcination conditions as opposed to under pure N_2.

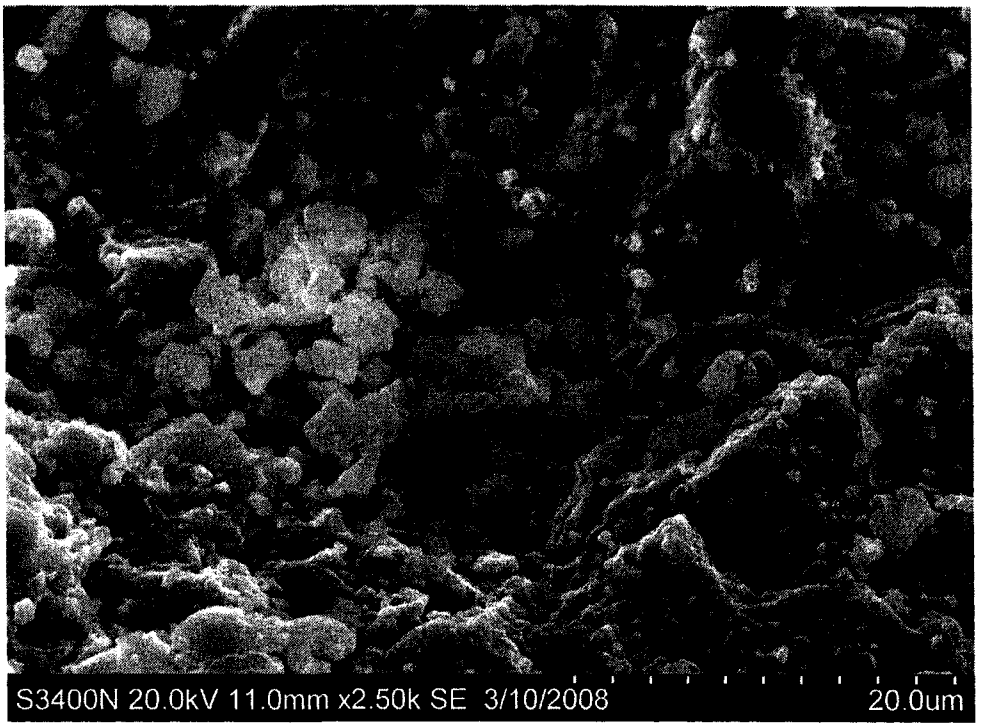

Figure 4.13: SEM image of a Havelock limestone particle after first calcination / carbonation cycle calcined at 915°C with N_2 and carbonated at 620°C with 8% CO_2, 21% H_2, 42% CO, 17% H_2O, and 12% N_2 – 20 micron scale.

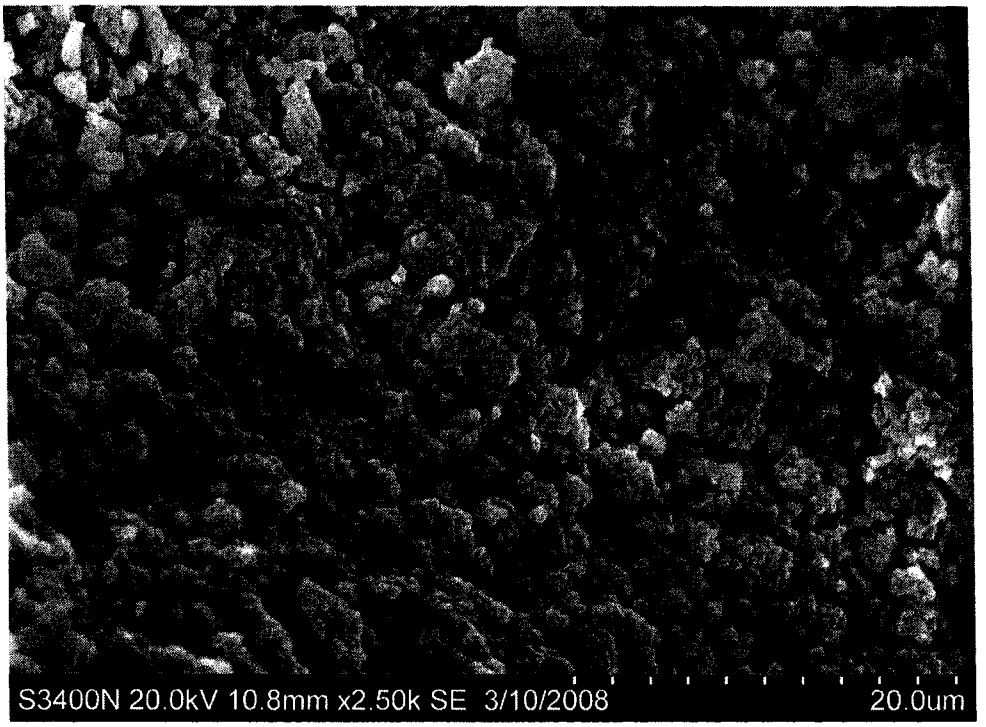

Figure 4.14: SEM image of a Havelock limestone particle after first calcination / carbonation cycle calcined at 915°C with 90% CO_2 and 10% N_2 and carbonated at 620°C with 8% CO_2, 21% H_2, 42% CO, 17% H_2O, and 12% N_2 – 20 micron scale.

To further support the work of Borgwardt (1989), it should be noted that the respective CaO conversions with and without CO_2 present during calcination for the first carbonation cycle (20 minutes) were 0.40 and 0.67. The decrease in CaO conversion can be associated with the reduction in microporosity where the bulk of conversion takes place especially during the first few calcination / carbonation cycles. As a final comparison, the effect of calcination temperature can be explored. The CaO conversions for the first calcination / carbonation cycle were 0.67 and 0.71 at calcination temperatures of 915 and 650°C respectively. This result is in agreement with the studies performed by Borgwardt (1989) and Silcox et al. (1989) who showed that an increase in calcination temperature resulted in an increase in the initial rate of CaO particle sintering. This increase in the rate of sintering, due to increased temperature and longer exposure at temperature, can be directly related to the decrease in CaO conversion.

4.2 – Naturally Occurring Dolomite – Newfoundland Dolomite

4.2.1 – Effect of Carbonation Feed Gas

As was discussed in Chapter 4.1.1, there has been significant research on the effect of CO_2 feed gas partial pressures on the reaction kinetics of the CaO-CO_2 reaction but little or none in the presence of H_2O, CO, or H_2. Thus, it is of particular interest to see if these gases have an effect on the carbonation reaction kinetics or sorbent deactivation.

As was the case with the naturally occurring limestone, dolomite showed an increase in intrinsic rate constant and initial rate of carbonation with the presence of CO and H_2 during carbonation as can been seen in Table 4.4. Once again it is reasonable to assume that this increase in rate is associated with a higher CO_2 concentration at the CaO sites via the water-gas shift reaction. It should be mentioned that during the initial calcination, the $MgCO_3$ in the dolomite calcines to MgO and the carbonation conditions employed here do not allow the MgO to recarbonate. MgO is a known water-gas shift catalyst (Han and Harrison, 1994) but, as was the case with limestone, it is expected that the increase in initial rate of carbonation is also partially due to the CaO acting as a shift catalyst.

Table 4.4: Intrinsic rate constants for 250-425 micron Newfoundland dolomite particles carbonated at 620°C for two different carbonation feed gas compositions.

Feed Gas Composition (vol%)	Total Pressure (atm)	Carbonation Temperature (°C)	r_0 (1/s)	k_s (mol/m^2.s.kPa)
8 CO_2, 21 H_2, 42 CO, 17 H_2O, 12 N_2	1	620	0.0016	9.17E-07
8 CO_2, 17 H_2O, 75 N_2	1	620	0.0015	8.41E-07

Figure 4.15 shows the CaO conversion of 250-425 micron Newfoundland dolomite particles calcined under pure nitrogen, carbonated with and without CO and H_2 over 10 calcination / carbonation cycles. Two major conclusions can be drawn from this figure. The first is that the presence of CO and H_2 during carbonation has little or no effect on the maximum carbonation conversion over repeated cycles and second is that the maximum conversion seems to remain relatively stable over 10 calcination /

carbonation cycles. As was the case with the limestone, it was expected that if the calcination conditions were identical (i.e., same feed gas, temperature, and time at temperature), then the presence of CO and H_2 during carbonation would not effect particle sintering or pore pluggage which is associated with a decrease in maximum conversion. On the other hand, it was shown that for limestone that the presence steam during carbonation had a large impact on the maximum CaO conversion plausibly related to the creation of many larger voids. Unfortunately, SEM images of dolomite samples carbonated without the presence of steam could not be obtained for comparison and based on work performed by (Li et al., 2005) dolomites with near identical chemical compositions showed large differences in maximum CaO conversion over repeated cycles. Thus, the effect of steam during carbonation cannot be observed as all carbonation feed gases in this work contain steam.

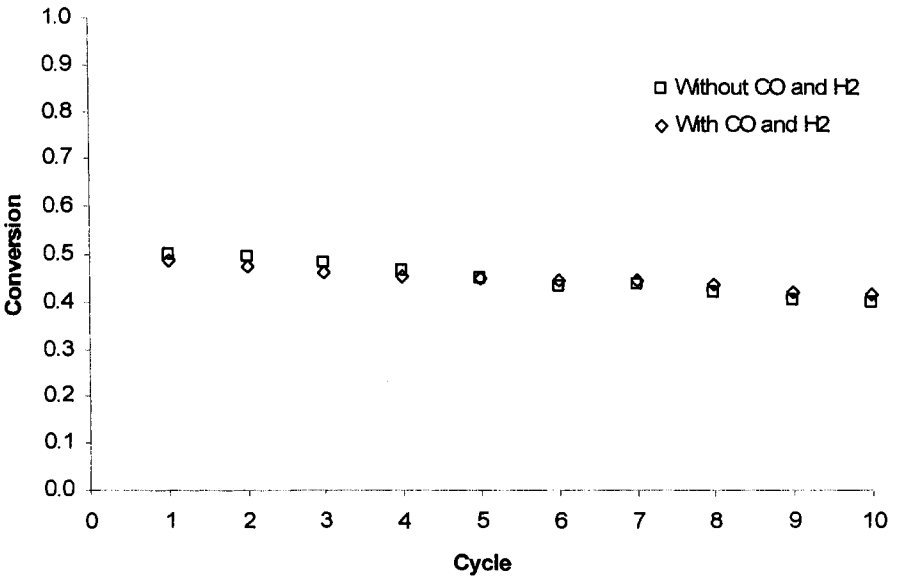

Figure 4.15: The decay in maximum carbonation conversion with the number of cycles for 250-425 micron Newfoundland dolomite particles calcined at 850°C with N_2 and carbonated at 620°C with and without the presence of CO and H_2.

As mentioned above, the maximum conversion seems to remain relatively stable, with a decrease in CaO conversion of only 0.10 over 10 cycles. This phenomenon can be explained by several factors. The first is that the inactive MgO contained in the calcined dolomite, which does not take part in the carbonation reaction, might hinder CaO sintering during calcination. In addition, the dolomite calcine provides more space for

the swelling solid product ($CaCO_3$), allowing for a higher ultimate conversion (Sun et al., 2008a). The final factor is related to a phenomenon occurring predominantly in dolomites known as decrepitation. The current belief is that decrepitation is a result of the pressure build-up of water within the lattice until it exceeds the mechanical strength of the particle resulting in a mini-explosion (McCauley and Johnson, 1991). This occurrence can be clearly seen in Figure 4.16 where the previously 250-450 micron range particle has been decrepitated into a series of smaller particles less than 200 microns in size. It is possible that this increase in the number of particles from decrepitation also increases the surface area due to the creation of larger pores/voids. As discussed in Chapter 4.1.1, that larger pores/voids are responsible for the majority of the CaO conversion as the microporosity is eliminated due to particle sintering over repeated cycles. Thus, explaining the relatively stable cyclic conversion, as larger pores/voids are not substantially affected by sintering or pore pluggage.

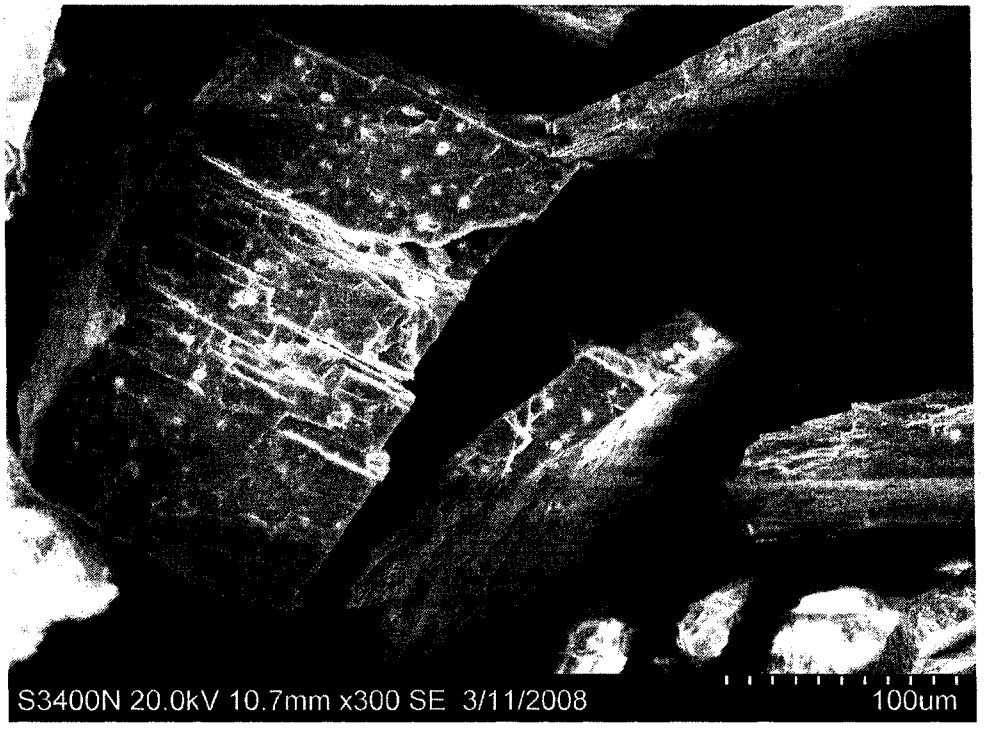

Figure 4.16: SEM image of a Newfoundland dolomite particle after decrepitation – 100 micron scale.

4.2.2 – Effect of Carbonation Temperature

As was the case with limestone, in order quantify the reaction kinetics and obtain the activation energy for the CaO-CO_2 reaction it is necessary to carbonate at several different temperatures. From the Arrhenius plots, the activation energies for the carbonation of 250-425 micron Newfoundland dolomite particles with and without CO and H_2 are 21.6 and 17.4 kJ/mol respectively. As described in Chapter 4.1.2, the increase in activation energy has been associated with the creation of CaO molecules forming intermediate complexes with CO and H_2O via the water-gas shift reaction. For comparison, the activation energy determined in the absence of CO and H_2 is close to within the level of uncertainty of the value determined by Sun et al. (2008b) which was 24 ± 6 kJ/mol for 38-45 micron Strassburg limestone particles.

From a practical point of view, it is important to determine if an increase or decrease in temperature has an impact on the maximum CaO conversion over repeated calcination / carbonation cycles. Figure 4.17 shows the decay in CaO conversion over 10 calcination / carbonation cycles for 4 temperatures ranging from 580 to 700°C with the presence of CO and H_2 during carbonation. As was the case with the naturally occurring limestone, the carbonation temperature does not significantly impact the maximum carbonation conversion over repeated cycles. In contrast, the absence of CO and H_2 during carbonation, depicted in Figure 4.18, shows a similar trend. As discussed in Chapter 4.2.1, the presumed water-gas shift reaction does not have a considerable impact on the rate of CaO carbonation. Therefore, for a 20 minute carbonation period it would be expected that for both carbonation feed gas compositions that the maximum cyclic conversion follow the same trend. Since there does not seem to be any correlation between the carbonation temperature and the maximum conversion (i.e., higher temperatures given a higher conversion), it can be assumed that the CaO particles have reached full conversion within the period and the associated variability must be related to the change in CaO composition and particle size from sample to sample, as discussed in Chapter 4.1.2.

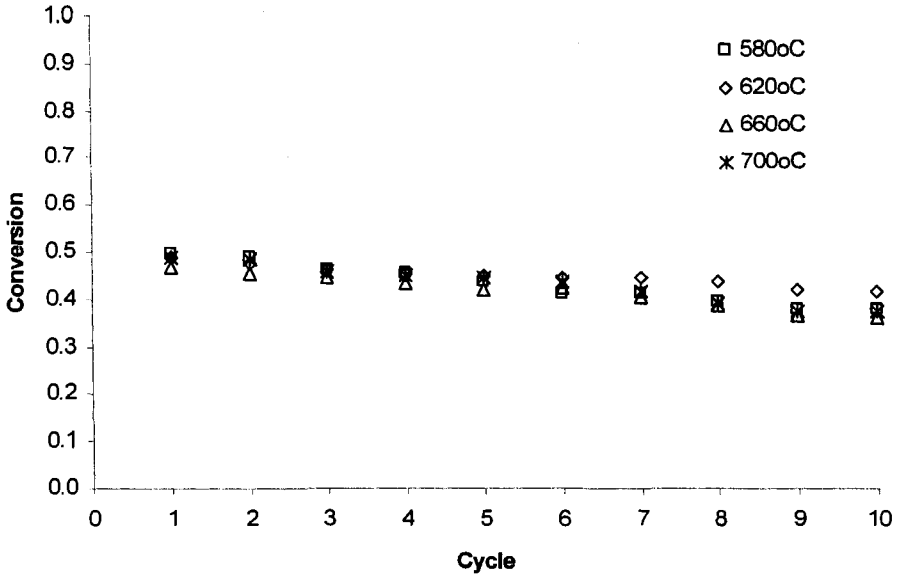

Figure 4.17: The decay in maximum carbonation conversion with the number of cycles for 250-425 micron Newfoundland dolomite particles calcined at 850°C with N_2 and carbonated at 4 temperatures with 8% CO_2, 21% H_2, 42% CO, 17% H_2O, and 12% N_2.

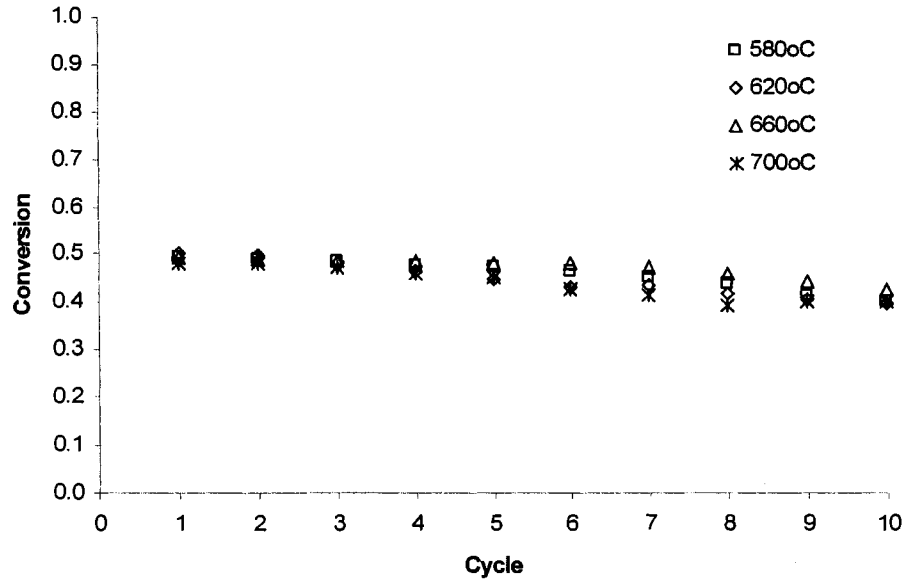

Figure 4.18: The decay in maximum carbonation conversion with the number of cycles for 250-425 micron Newfoundland dolomite particles calcined at 850°C with N_2 and carbonated at 4 temperatures with 8% CO_2, 17% H_2O, and 75% N_2.

4.2.3 – Effect of Calcination Feed Gas

As noted in Chapter 4.1.3, the addition of CO_2 during calcination has an adverse effect on CaO conversion of limestone due to accelerated particle sintering and pore closure. As well, the presence of CO_2 had a significant impact on the reaction kinetics, indicated by a drastic decrease in the initial rate of carbonation. Thus, it is of interest to determine the effect of calcination feed gas conditions on the carbonation kinetics and CaO conversion for a naturally occurring dolomite. Table 4.5 lists the initial rates and rate constants of the CaO-CO_2 reaction at 620°C for 250-425 micron Newfoundland dolomite particles calcined under CO_2 / N_2 and pure N_2.

Table 4.5: Initial rates and rate constants for 250-425 micron Newfoundland dolomite particles carbonated at 620°C with 8% CO_2, 21% H_2, 42% CO, 17% H_2O, and 12% N_2 for two different calcination feed gas compositions.

Feed Gas Composition (vol%)	Total Pressure (atm)	Calcination Temperature (°C)	r_0 (1/s)	k_s (mol/m^2.s.kPa)
90 CO_2, 10 N_2	1	915	0.0021	1.18E-06
100 N_2	1	915	0.0022	1.21E-06

Unlike the calcitic limestone, it is evident that the addition of CO_2 during calcination has a little or no effect on the initial rate of carbonation as can be seen in Table 4.5. Under a 90 % CO_2 atmosphere the initial rate of carbonation is only approximately 5 percent lower than with pure N_2. As mentioned in Chapter 4.2.1, the effect of decrepitation is believed to decrease the microporosity and increase the number of larger voids / pores where the majority of the CaO conversion will now take place. Since it is known that during sintering, necks develop between adjacent grains affecting only the microporosity, it is reasonable to believe that the rate of carbonation would not be influenced by the presence of CO_2 during calcination. This can be seen more clearly in Figures 4.19 and 4.20 which show that the presence of CO_2 during calcination has no significant impact on the surface morphologies. To further support the argument that the majority of the CaO conversion is taking place in the larger voids / pores is that the CaO conversion with and without CO_2 presence during calcination for the first carbonation cycle were 0.47 and 0.48 respectively. Since the particle sintering is not affecting the

larger voids / pores, the nascent CaO surface area should remain unchanged resulting in the near identical conversions under varying calcination feed gas conditions.

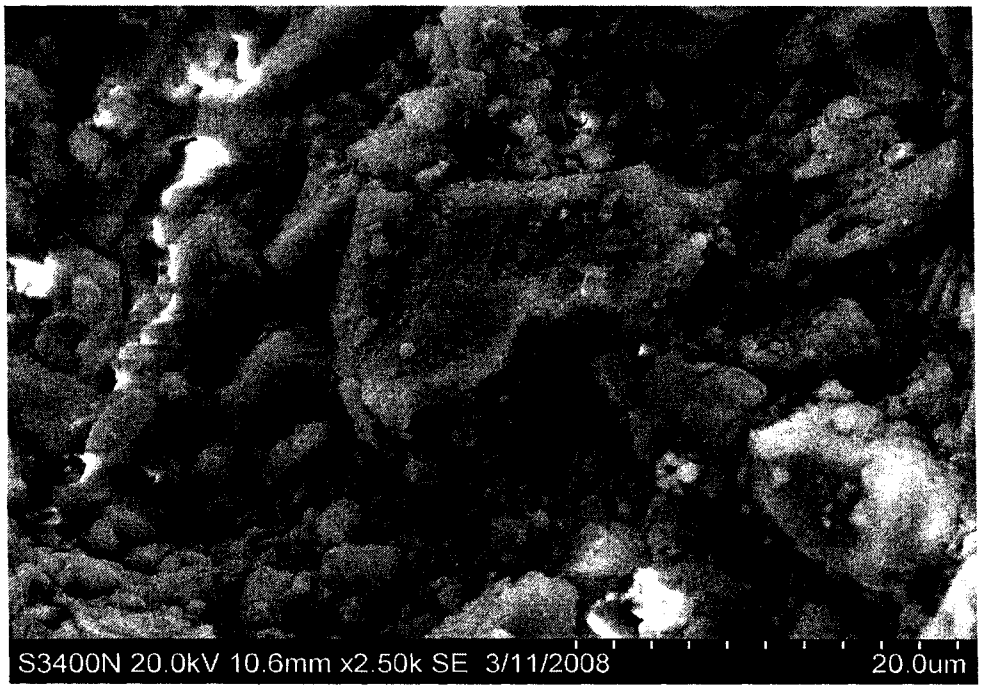

Figure 4.19: SEM image of a Newfoundland dolomite particle after first calcination / carbonation cycle calcined at 915°C with N_2 and carbonated at 620°C with 8% CO_2, 21% H_2, 42% CO, 17% H_2O, and 12% N_2 – 20 micron scale.

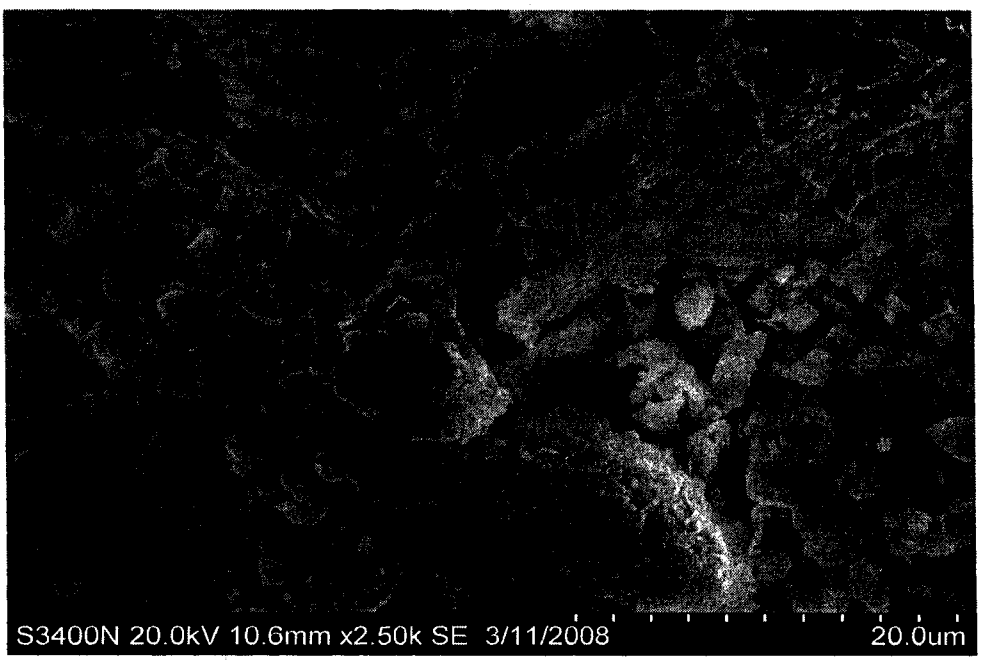

Figure 4.20: SEM image of a Newfoundland dolomite particle after first calcination / carbonation cycle calcined at 915°C with 90% CO_2 and 10% N_2 and carbonated at 620°C with 8% CO_2, 21% H_2, 42% CO, 17% H_2O, and 12% N_2 – 20 micron scale.

As a final point, the effect of calcination temperature on CaO conversion should be explored. The conversions for the first calcination / carbonation cycle were 0.48 and 0.49 at calcination temperatures of 915 and 650°C respectively. As expected, the conversions are nearly identical, once again indicating that sintering does not impact the CaO conversion for the Newfoundland dolomite particles.

4.3 – Comparison of Calcium Oxide based Sorbents

For both the naturally occurring limestone and dolomite, the presence of CO and H_2 during carbonation has been shown to have significant impact on the initial rate of carbonation and rate constant. This rate enhancement has been attributed to an increase in the partial pressure of CO_2 at the CaO surface via the water-gas shift reaction. In the case of the dolomite, it is known that the water-gas shift can take place as the calcined dolomite contains MgO, a recognized water-gas shift catalyst. Thus, it is of interest to compare the increase in initial rate with and without CO and H_2 between limestone and dolomite.

For limestone, the increase in initial rate via the addition of the water-gas shift reaction is approximately 70.6 percent and for dolomite approximately 9.1 percent, both carbonated at 620°C. From this result it appears that the limestone is more affected by the presence of the water-gas shift reaction. This result can be interpreted in two separate ways. The first is that the CaO surface sites act as better water-gas shift catalyst than the MgO surface sites and the second is related to the differences in pore structure between the limestone and dolomite. Although it is plausible that the CaO surface sites act as a better catalyst, this seems unlikely. The worked performed by Han and Harrison (1994) showed that even though the water-gas shift reaction does occur in the presence of limestone and dolomite, the dolomite was in fact the superior catalyst. Thus, the effect of the water-gas shift reaction is most likely related to the differences in pore structure. As mentioned in Chapters 4.1 and 4.2, there is a great distinction in where the CaO conversion takes place for the first few cycles for limestone and dolomite. For the limestone, the initial conversion takes place principally in the micropores where as for the dolomite, it is appears to take place mainly in the larger voids / pores created by particle decrepitation (McCauley and Johnson, 1991). Looking at Figure 4.21 (pore volume distribution for BET analysis), there are in fact a greater proportion of larger pores lying in the mesoporous / macroporous region. Interestingly, the dolomite particles have a comparable differential pore volume lying between the pore range of 2 and 6 nm. As discussed in Chapter 4.1, it is well known that initially high cyclic carbonation conversion of limestones is due to the majority of carbonation taking place in the

micropores which is eliminated by repeated calcination. From Figure 4.22, the dolomite does not show a significant decrease in maximum conversion over the first few cycles, thus, it can be inferred that the majority of CaO conversion takes place in the larger voids / pores and the surface area within the micropores is related mainly to the inactive MgO.

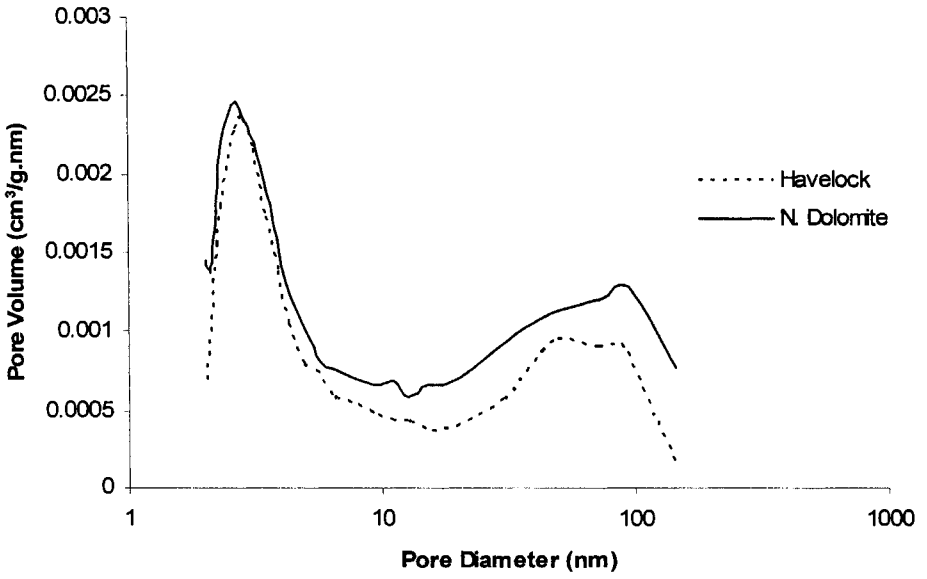

Figure 4.21: Pore size distribution of 250-425 micron Havelock limestone and Newfoundland dolomite particles calcined at 850°C with N_2.

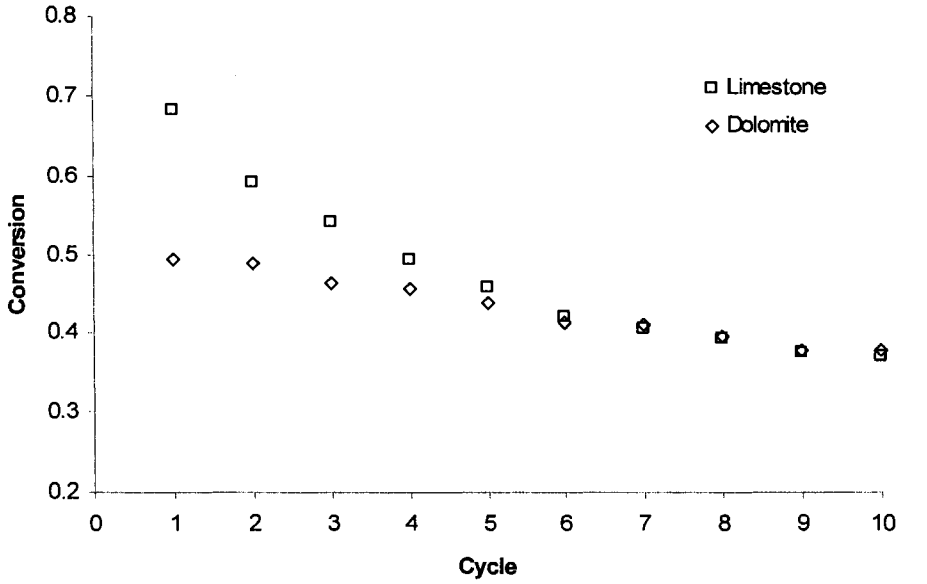

Figure 4.22: The decay in maximum carbonation conversion with the number of cycles for 250-425 micron calcium oxide based sorbent particles calcined at 850°C with N_2 and carbonated at 620°C with 8% CO_2, 21% H_2, 42% CO, 17% H_2O, and 12% N_2.

Based on the above conclusion, since the concentration gradient from the bulk gas to the nascent CaO sites in the larger voids / pores would be significantly lower than in the micropores, it appears to be reasonable that the increase in CO_2 concentration via the water-gas shift would have a proportional smaller increase in the total CO_2 concentration at the surface sites. Therefore, the increase in rate of carbonation would be proportional lower. This phenomenon can be observed by comparing the slopes with and without CO and H_2 for limestone as compared to dolomite as can be seen in Figure 4.1 and 4.23, respectively. It should be noted that there must exists some CaO surface sites within the microporosity as indicated by the minor decrease in maximum conversion over 10 cycles.

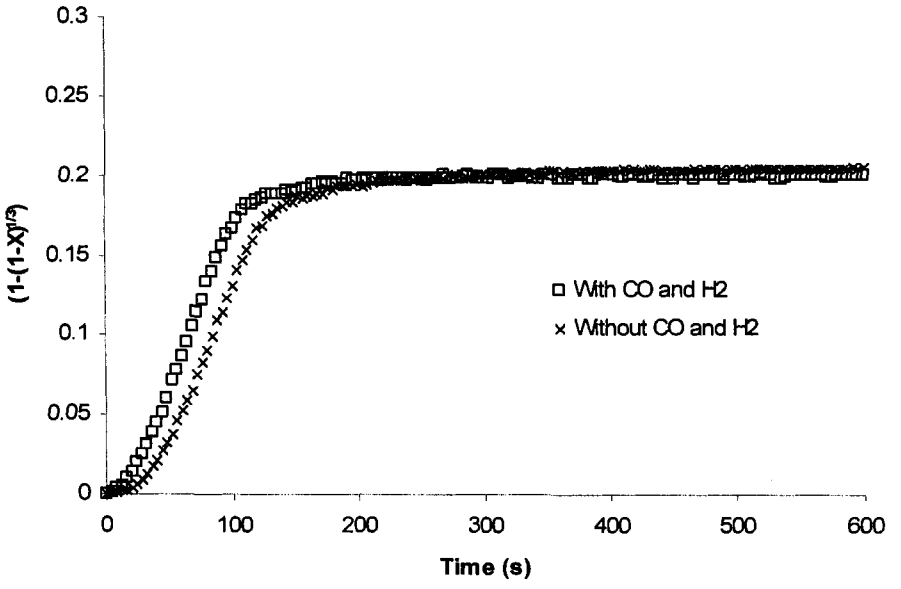

Figure 4.23: Grain model plot for 250-425 micron Newfoundland dolomite particles calcined at 850°C with N_2 and carbonated at 620°C with and without CO and H_2.

From Figure 4.22, it can bee seen that after 6 cycles the maximum CaO conversion for both limestone and dolomite are essentially identical. Although the conversions may be similar, it is of interest to compare the capture ability for limestone and dolomite derived sorbents. Since the molar density of CaO in dolomite derived calcines is significantly lower than for limestone derived calcines, the capture ability of limestone is higher than for an equal mass of dolomite. As was indicated in Chapters 4.1.2 and 4.2.2, the activation energy for limestone was somewhat higher (approximately 70.7 %) than dolomite. This result is consistent with the work performed by Kyaw et al.

(1996) and Sun et al. (2008b). According to Sun et al., the difference in due to the structure related difference during nucleation or formation of the solid product. For the $CaO-CO_2$ reaction with swelling solid product, the rate of reaction is related to both a chemical and mechanical energy change where the mechanical energy is related to the strain energy between different grains. Young (1996) showed that during the nucleation stage the solid structure might influence the overall free energy change. Thus, for the reaction to occur not only the energy barrier involved with chemical energy must be reached but also a structure related mechanical barrier needs to be overcome. Since dolomite contains a significant amount of MgO acting as impurity, it is likely to have relatively low strain energy, resulting in lower apparent activation energy than limestone. As well, it was pointed out by Young (1966) that during the incipient nucleation stage, the germ nucleus is "situated at regions of disorders, such as points of emergence of dislocations, vacancies, interstitial or impurity clusters." The reactant at these points must re-crystallize more readily than on a normal surface because the fewer bonds per ion need to be broken. Since it is known that the magnesium in dolomite causes dislocations at full calcination, it is plausible that this rational is responsible for the lower energy barrier for dolomite and hence, a lower activation energy.

4.4 – Parametric Analysis of Carbonator Moving Bed Reactor Model

Axial profiles of bed temperature, percent CO_2 concentration, carbonation conversion of CaO, and total bed pressure are determined via the moving bed reactor model described in Chapter 3.3 by varying the inlet CaO and feed gas superficial velocities, the inlet temperature, and the number of calcination / carbonation cycles. The moving bed simulation has been performed for the case where Havelock CaO particles are introduced co-currently with the syngas feed gas into a cylindrical tube reactor with an inner diameter of 0.1 m and a total bed length of 0.5 m.

4.4.1 – Effect of CaO Inlet Superficial Velocity

Figures 4.24 to 4.27 show the effect of varying CaO inlet superficial velocities on the axial distributions of the bed temperature, the percent CO_2 composition, the CaO carbonation conversion, and the total bed pressure respectively. The CaO superficial velocities used for the simulation are 0.0005, 0.0008, 0.0010, and 0.0015 m/s, which in terms of mass flow rates, corresponds to 0.38, 0.61, 0.76, and 1.15 kg/min and retention times of 16.6, 10.4, 8.3, and 5.6 min, respectively.

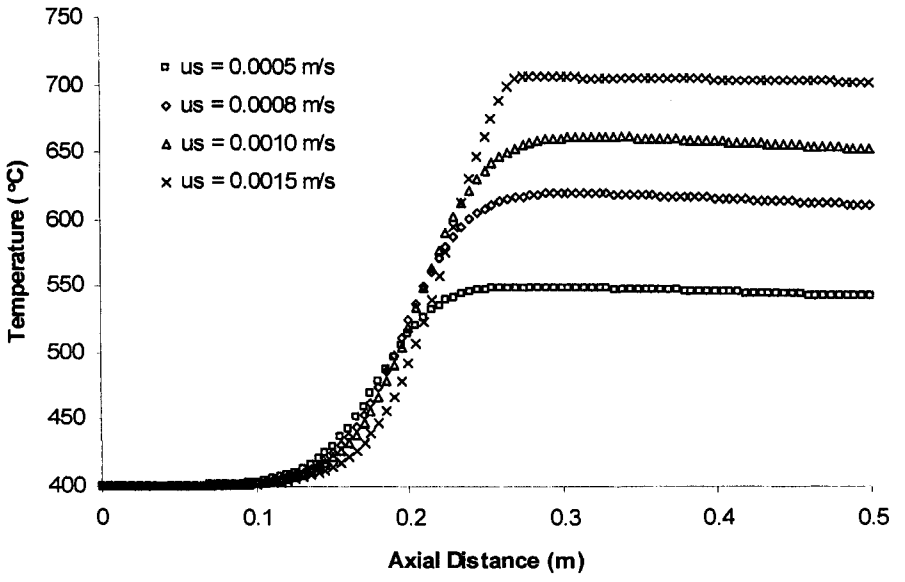

Figure 4.24: Effect of CaO inlet superficial velocity on the axial distribution of the bed temperature (8% CO_2, inlet temperature = 400°C, inlet pressure = 1 atm, feed gas superficial velocity = 5 m/s, 1st carbonation cycle).

As expected, Figure 4.24 shows that as the carbonation reaction proceeds over the reactor length, the bed temperature also increases until it reaches a point where complete CaO carbonation is achieved. After this point, the bed temperature begins to slowly drop due to heat lost through the reactor wall, as the wall temperature is assumed to remain constant at 400°C. The CaO carbonation conversion as a function of the axial reactor distance can be seen in Figure 4.25. Returning to Figure 4.24, as the inlet CaO superficial velocity increases so does the bed temperature as a result of the increased release of heat from the exothermic carbonation reaction of more CaO. Unfortunately, as the CaO feed velocity increase beyond 0.0010 m/s the increase in bed temperature results in a value of $C_{CO_2,eq}$ close to that in the bulk gas stream limiting the carbonation conversion which can be clearly observed in Figure 4.25. Thus, based on the limited throughput of CaO, the resulting amount of CO_2 removal is also restricted as shown in Figure 4.26.

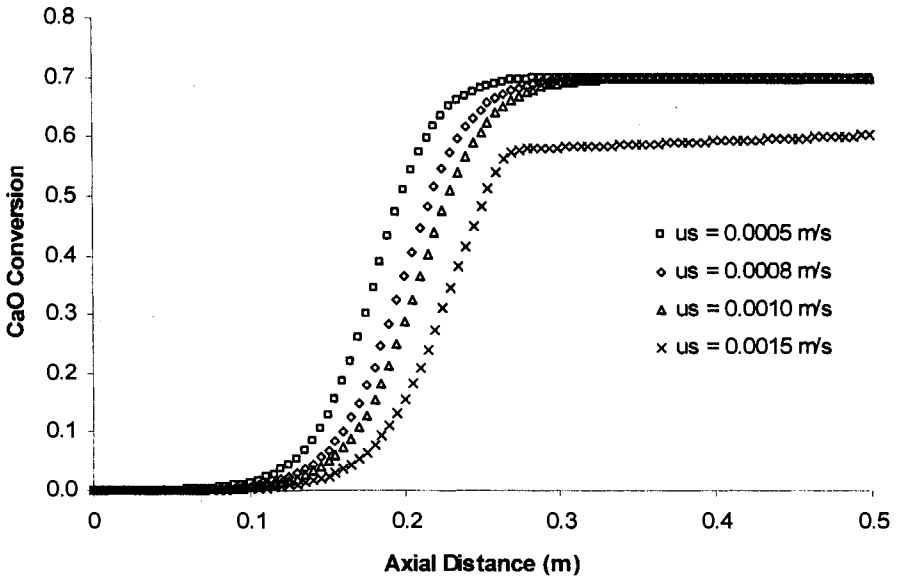

Figure 4.25: Effect of CaO inlet superficial velocity on the axial distribution of the CaO carbonation conversion (8% CO_2, inlet temperature = 400°C, inlet pressure = 1 atm, feed gas superficial velocity = 5 m/s, 1st carbonation cycle).

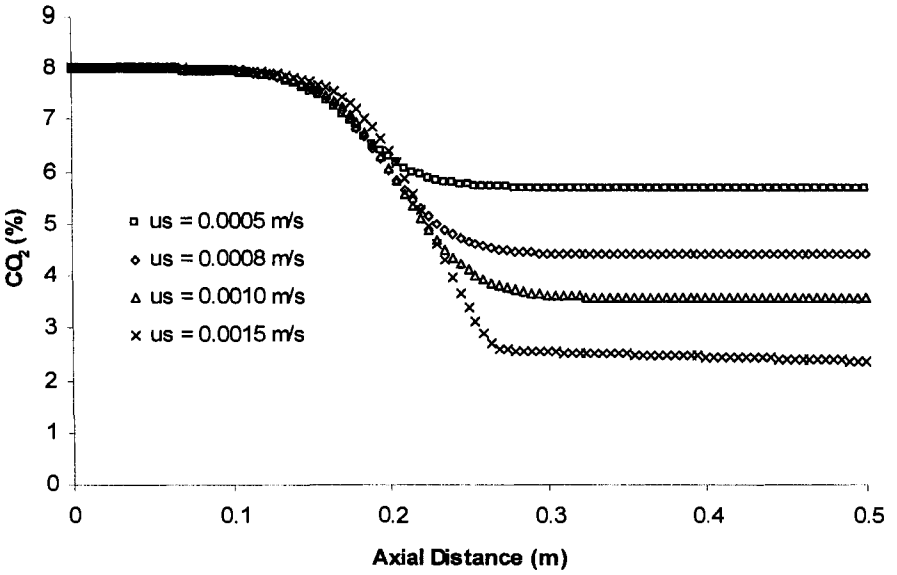

Figure 4.26: Effect of CaO inlet superficial velocity on the axial distribution of the percent CO_2 composition (8% CO_2, inlet temperature = 400°C, inlet pressure = 1 atm, feed gas superficial velocity = 5 m/s, 1st carbonation cycle).

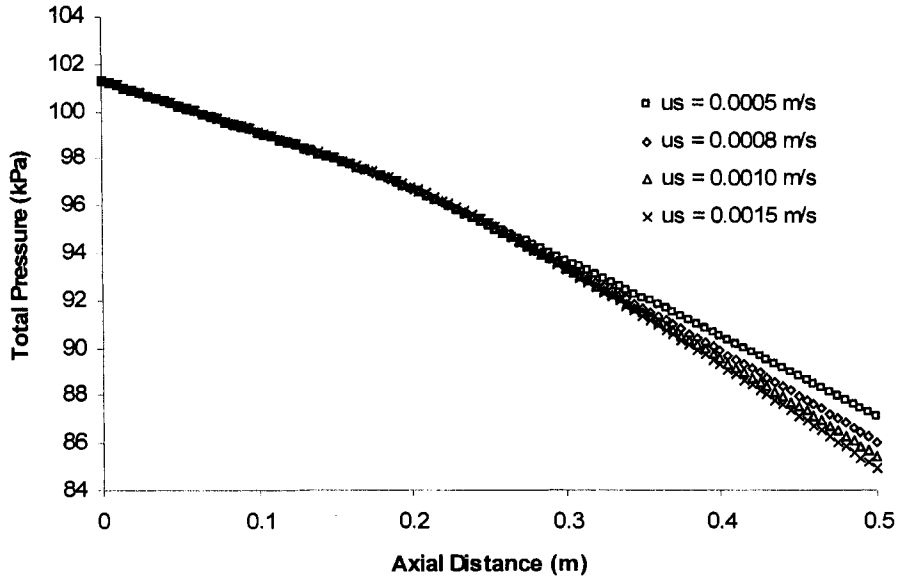

Figure 4.27: Effect of CaO inlet superficial velocity on the axial distribution of the total pressure (8% CO_2, inlet temperature = 400°C, inlet pressure = 1 atm, feed gas superficial velocity = 5 m/s, 1st carbonation cycle).

Although, the CO_2 removal can be slightly improved by increasing the CaO feed rate (resulting from more solids to absorb heat), this results in inefficient usage of the cyclic capture capability of the CaO particles. Due to significant changes in particle

porosity during calcination (Chapter 4.1), the capture capability drops rapidly over the first few cycles (30-40%). Therefore, for the process to be considered economical (minimizing the necessity for fresh CaO makeup) it is of great importance that the utilization of the capture capability be maximized. As anticipated, there is an increased pressure drop over the reactor length with increasing CaO inlet feed rate as the added heat release from carbonation increases the gas superficial velocity. From this result it can be deduced that the reactor pressure drop is more sensitive to changes in gas superficial velocity due to increases in bed temperature than to the decrease in CO_2 concentration.

4.4.2 – Effect of Feed Gas Superficial Velocity

As was the case with the CaO inlet superficial velocity, it is of particular interest to investigate the effect of differing feed gas superficial velocities on the axial distributions of the bed temperature, the percent CO_2 concentration, the CaO carbonation conversion, and the total bed pressure. The feed gas superficial velocities used for the simulation are 3, 5, 8, and 10 m/s, which in terms of volumetric flow rates, corresponds to 34.4, 57.4, 91.8, and 114.7 Nm^3/h, respectively. Figure 4.28 shows the axial distribution of the percent CO_2 concentration with varying feed gas superficial velocities. As predicted, since the CaO superficial velocity remains constant, a lower outlet CO_2 concentration can be achieved by decreasing the feed gas superficial velocity. Unfortunately, as was the case with the CaO superficial velocity, there is a significant limitation on the practical range of feed gas superficial velocities. At the upper limit, 10 m/s, the decrease in CO_2 composition is only approximately 1.56 % (19% CO_2 capture) resulting in inefficient usage of the CaO capture capability, due to an inadequate gas residence time and increase axial distance for gas heating, as can be seen in Figure 4.29. At the lower limit, 3 m/s, the CO_2 capture is considerably improved, 73 %, but due to a lower flow rate the gas stream is insufficient for heat removal generated by the carbonation reaction. This causes the bed temperature, seen in Figure 4.30, to increase to over 700°C resulting in a value of $C_{CO_2,eq}$ close to that in the bulk gas stream stifling the carbonation reaction. As well, this phenomenon leads to only a 77 % usage of the total possible CaO conversion. Thus, the optimal feed gas superficial velocity lies between 3

and 5 m/s to both maximize the CaO conversion while also minimizing the outlet CO_2 gas composition.

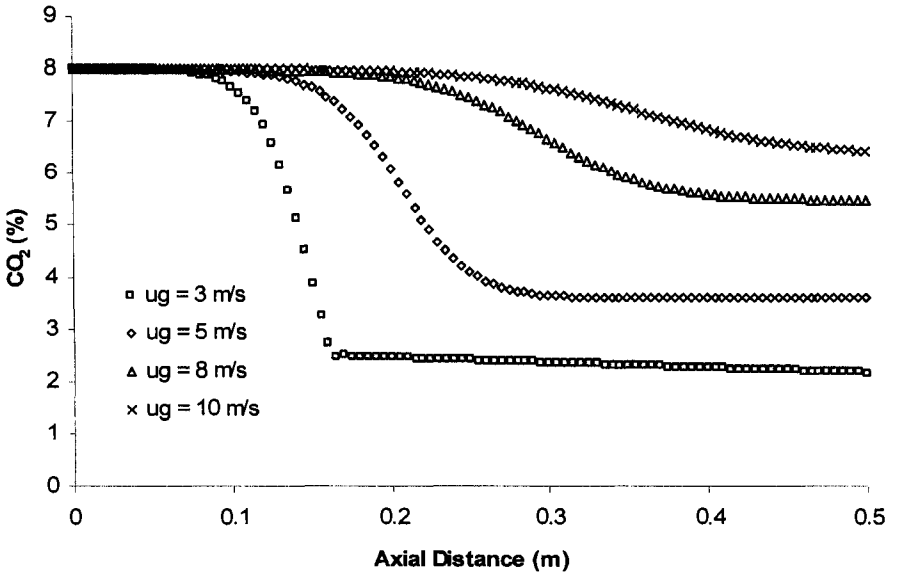

Figure 4.28: Effect of feed gas superficial velocity on the axial distribution of the percent CO_2 composition (8% CO_2, inlet temperature = 400°C, inlet pressure = 1 atm, CaO inlet superficial velocity = 0.0010 m/s, 1st carbonation cycle).

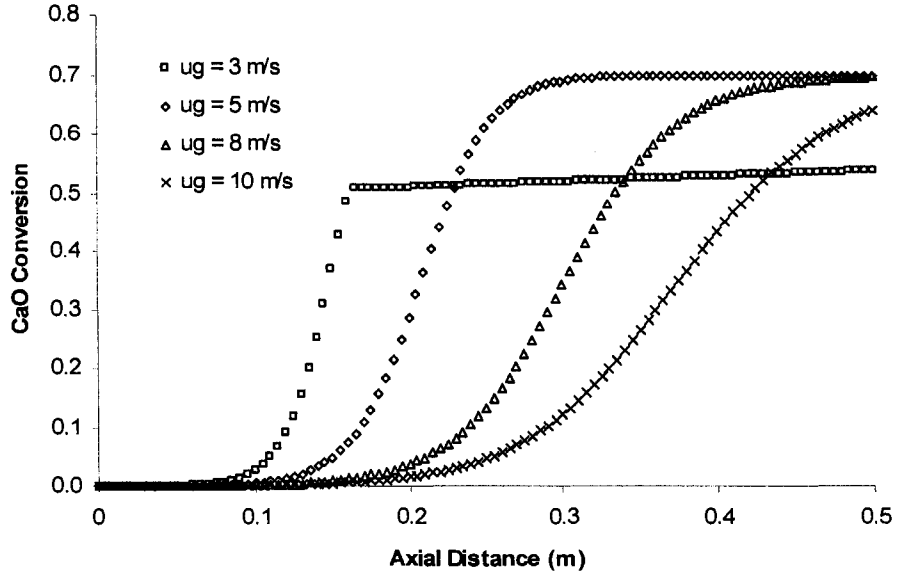

Figure 4.29: Effect of feed gas superficial velocity on the axial distribution of the CaO carbonation conversion (8% CO_2, inlet temperature = 400°C, inlet pressure = 1 atm, CaO inlet superficial velocity = 0.0010 m/s, 1st carbonation cycle).

As a final note, the pressure drop over the reactor length has been determined and as anticipated the pressure drop increases dramatically with increasing feed gas superficial velocity as the drop in pressure is directly related to the square of the gas velocity. Over the range of superficial velocities, 3 to 10 m/s, the associated pressure drops are 7.7 to 56.3 kPa, respectively.

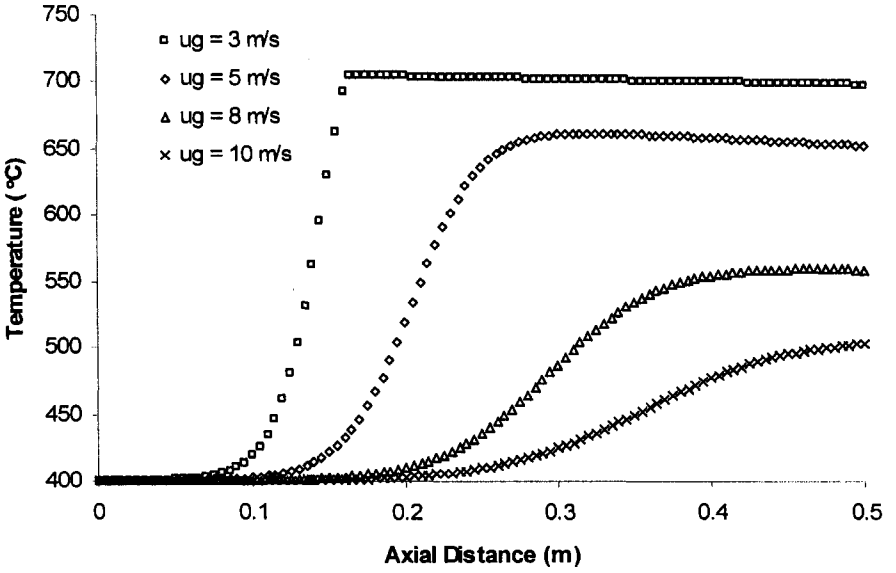

Figure 4.30: Effect of feed gas superficial velocity on the axial distribution of the bed temperature (8% CO_2, inlet temperature = 400°C, inlet pressure = 1 atm, CaO inlet superficial velocity = 0.0010 m/s, 1st carbonation cycle).

4.4.3 – Effect of Inlet Temperature

As discussed in the preceding sections, the axial distribution in bed temperature has a considerable impact on the overall effectiveness for the capture of CO_2 via CaO carbonation. Therefore, it is important to examine the effect of inlet temperature on the axial distributions of the bed temperature, the percent CO_2 concentration, the CaO carbonation conversion, and the total bed pressure. The inlet temperatures used for the simulation are 400, 405, 425, and 450°C with an associated CaO inlet superficial velocity of 0.10 cm/s and feed gas volumetric flow rate of 57 Nm^3/h.

From Figure 4.31, it can be observed that the inlet feed gas/CaO temperature has a dramatic effect on the axial distribution of the bed temperature. In the case of an inlet temperature of 400°C, the increase in temperature due to carbonation takes place closer to the outlet of the reactor and as the inlet temperature is increased the reaction moves

closer to the inlet of the reactor (Figure 4.32). This can be explained by the reaction kinetics of the carbonation reaction. At a temperature of 400°C, the carbonation reaction proceeds extremely slowly and begins to accelerate only as the release of heat from carbonation raises the bed temperature. As the inlet temperature is increased, the reaction is shifted into a more favourable kinetic region, allowing for the carbonation to occur closer to the reaction inlet.

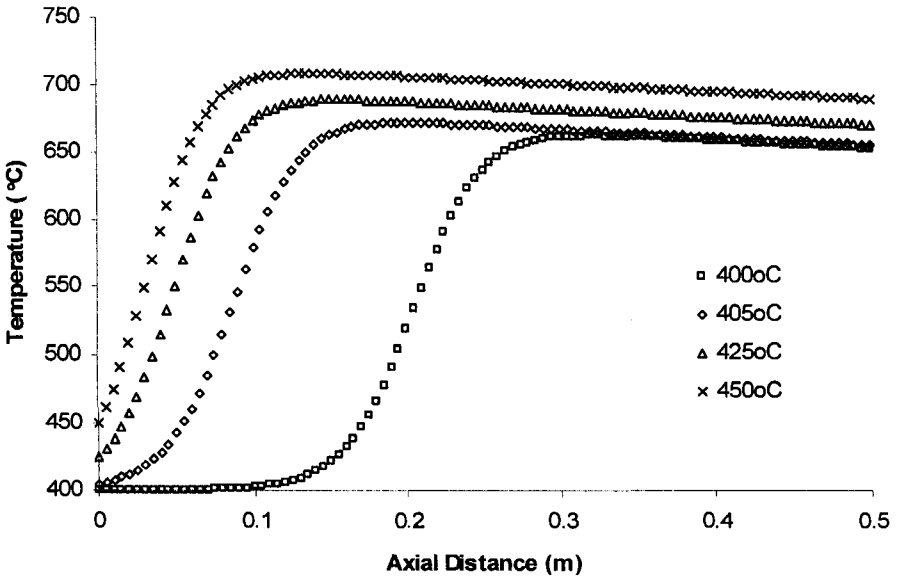

Figure 4.31: Effect of inlet temperature on the axial distribution of the bed temperature (8% CO_2, inlet pressure = 1 atm, CaO inlet superficial velocity = 0.0010 m/s, feed gas volumetric flow rate = 57.4 Nm^3/h, 1st carbonation cycle).

From a particle point of view, the temperature range of 400 to 450°C would represent the only feasible inlet temperatures for this process. At the low end, a temperature below 400°C would result in extremely unfavorable reaction kinetics where the CaO carbonation conversion would be close to zero or very minimal. At the high end, as was the case with low feed gas or high CaO superficial velocities, an inlet temperature above 450°C would result in a bed temperature higher than 700°C and an associated value of $C_{CO_2,eq}$ close to that of the bulk gas stream. This is turn would limit the rate of carbonation leading to a CaO conversion below its maximum potential. It should be noted that there is an associated error with the determination of the carbonation reaction kinetics at lower temperatures as the experimental kinetic data does cover

temperatures as low as 400°C. Thus, the kinetic constants were calculated via extrapolation of the non-linear regression of experimental data.

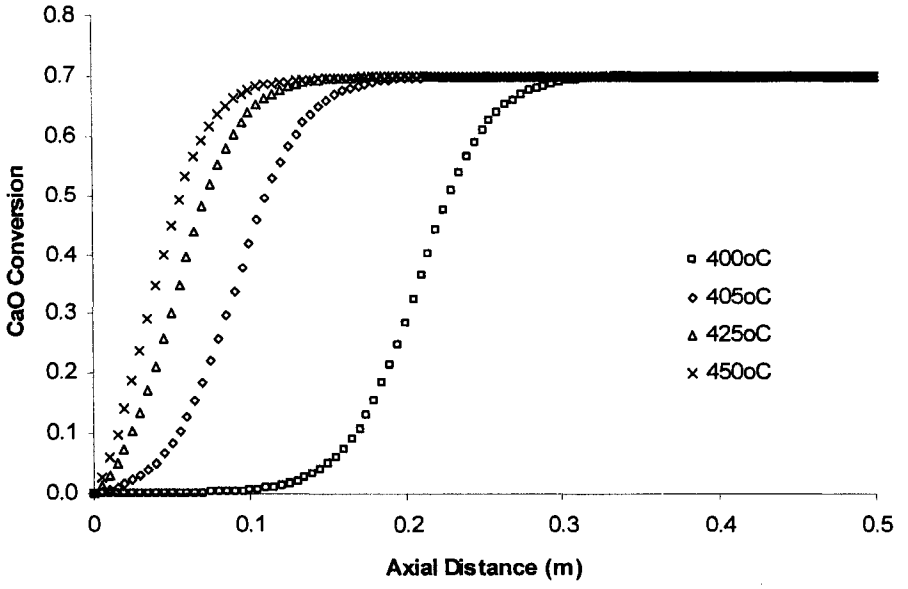

Figure 4.32: Effect of inlet temperature on the axial distribution of the CaO carbonation conversion (8% CO_2, inlet pressure = 1 atm, CaO inlet superficial velocity = 0.0010 m/s, feed gas volumetric flow rate = 57.4 Nm^3/h, 1st carbonation cycle).

Not shown are plots of CO_2 composition and total system pressure versus axial reactor distance. Based on Figure 4.32, the CaO conversion is complete and since the gas and CaO feed rates are identical for all inlet temperatures, the resulting CO_2 composition at the reactor outlet remains constant at 3.32 %. As for the system pressure drop, it stands to reason that as the inlet temperature is increased so to does the gas superficial velocity and hence the pressure drop. Over the range of inlet temperatures, 400 to 450°C, the associated pressure drops are 15.9 to 19.8 kPa, respectively.

4.4.4 – Effect of Calcination / Carbonation Cycle Number

The previous sections have examined the impact of CaO feed rate, feed gas superficial velocity, and inlet temperature on the axial distributions of the bed temperature, the percent CO_2 concentration, the CaO carbonation conversion, and the total bed pressure. In all the cases, the CaO particles have only undergone an initial calcination and, as discussed in Chapter 4.1, subsequent calcination / carbonation cycles

dramatically decrease the maximum cyclic carbonation conversion as can be seen in Figure 4.40.

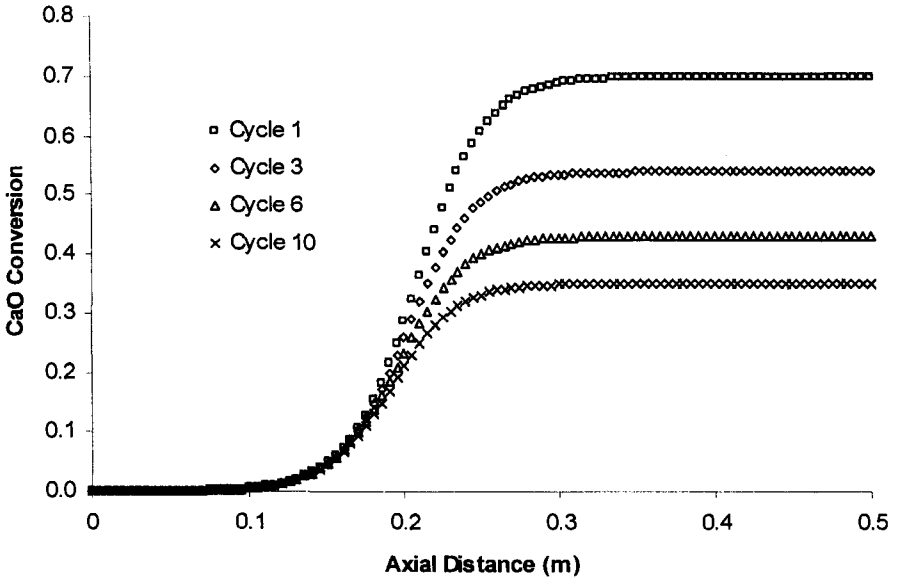

Figure 4.33: Effect of cycle number on the axial distribution of the CaO carbonation conversion (8% CO_2, inlet temperature = 400°C, inlet pressure = 1 atm, CaO inlet superficial velocity = 0.0010 m/s, feed gas volumetric flow rate = 57.4 Nm^3/h).

It should be noted that the decrease in maximum cyclic carbonation conversion is more pronounced over the first few cycles, decreasing from 0.70 to 0.54 and 0.43 to 0.35 from cycles 1 to 3 and cycles 6 to 10, respectively. As expected, this decrease in CaO conversion causes a reduction in the total capture of CO_2 from the feed gas stream. At a constant CaO feed superficial velocity of 0.10 cm/s and feed gas volumetric flow rate of 57.4 Nm^3/h, the CO_2 composition at the reactor outlet rises from 3.58 to 5.68 % from cycle 1 to 10, respectively. Thus, it becomes apparent that for the process to maintain its efficiency the spent CaO particles must be removed after a set number of calcination / carbonation cycles and a makeup stream of fresh $CaCO_3$ added to the process to boost the removal of CO_2. Looking at Figure 4.34, the maximum bed temperature drops significantly with increasing calcination / carbonation cycles which is anticipated because of a decline in heat release associated to carbonation. Assuming the addition of fresh $CaCO_3$ and the removal of deactivated CaO, it stands to reason that the maximum bed temperature would be lower than maximum bed temperature for the first cycle, approximately 660°C. Since the carbonation reaction is limited by $C_{CO_2,eq}$, which directly

related to the bed temperature, the feed gas superficial velocity could be decrease (assuming the CaO feed rate remains constant) improving the reduction in CO_2 composition at the reactor outlet. At this point it should be mentioned that one method for improving the overall efficiency of the process (i.e., minimize the outlet CO_2 composition) would be to add a cooling jacket (or another cooling system, e.g., tube bundles) around the entrance of the reactor, where the majority of the carbonation takes place. Thus, the feed gas flow rate could be adjusted to obtain any desirable CO_2 outlet composition while eliminating the necessity of high superficial velocities for the convective heat removal.

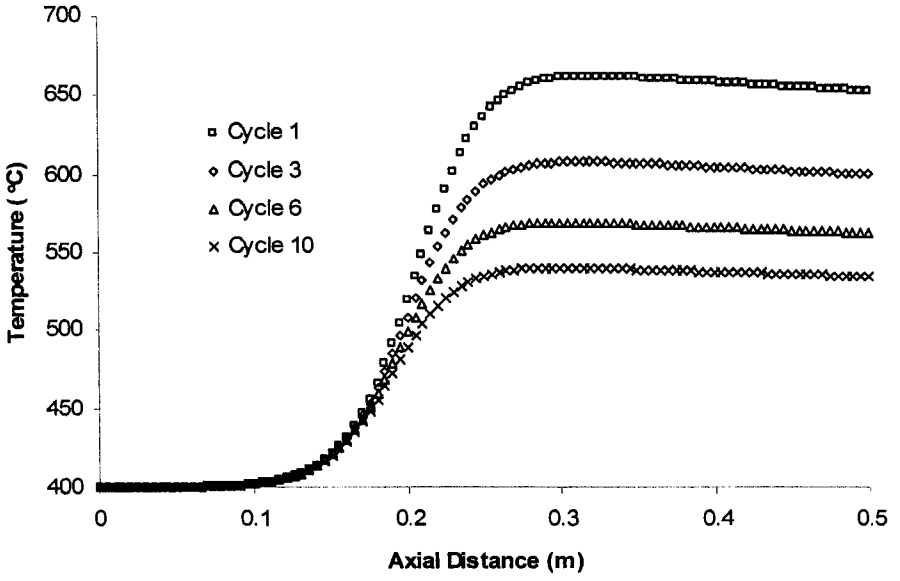

Figure 4.34: Effect of cycle number on the axial distribution of the bed temperature (8% CO_2, inlet temperature = 400°C, inlet pressure = 1 atm, CaO inlet superficial velocity = 0.0010 m/s, feed gas volumetric flow rate = 57.4 Nm^3/h).

Not shown is the plot total system pressure versus axial reactor distance. Since the total quantity of CO_2 carbonated from cycle to cycle decreases, it stands to reason that the average bed temperature will decrease leading to a lower gas superficial velocity and hence a lesser pressure drop. Over the range of 1 to 10 calcination / carbonation cycles, the associated pressure drops are 15.9 to 14.0 kPa, respectively.

Chapter 5 – Conclusions and Recommendations

This work aimed at determining the effect of gasification syngas on the carbonation reaction kinetics for two naturally occurring calcium oxide based sorbents, developing a suitable moving bed carbonator reactor model, and evaluating the reactor model under a multitude of operating conditions.

The carbonation reaction kinetics were quantified based on the use of a grain model that is applied to the initial stage of carbonation where the reaction is under kinetic control. Experiments were performed via the use of a thermogravimetric analyzer whereby small samples (24-26 mg) of naturally occurring CaO based sorbents, specifically one limestone and one dolomite, were exposed to a feed gas stream containing CO_2 at elevated temperatures (580-700°C). Through experiments performed with and without the presence of CO and H_2 during carbonation, it was possible to determine if the intrinsic rate constant for the CaO-CO_2 reaction was affected by gasification syngas.

At a reaction temperature of 620°C, it was determine that the presence of CO and H_2 caused an increase in initial rate of approximately 70.6 percent for limestone and 9.1 percent for dolomite. The increase in rate was attributed to the CaO surface sites catalyzing the water-gas shift reaction increasing the local CO_2 concentration. As well, the water-gas shift reaction was assumed to be responsible for the increase the activation energy from 29.7 to 60.3 kJ/mol for limestone and 17.4 to 21.6 kJ/mol for dolomite based on the formation of intermediate complexes. Structural differences between the two sorbents are believed to be accountable for the difference in activation energies.

Changes in the porosity due to particle sintering during calcination have been credited with the initial rapid decrease in cyclic CaO maximum conversion for limestone particles whereas the presence of steam during carbonation has been shown to improve the long term maximum conversion in comparison to previous studies without steam present. On the other hand, the dolomite showed a minimal decrease in CaO maximum conversion over repeated cycles as the majority of the carbonation was inferred to take place in the larger pores / voids which is less susceptible to particle sintering and pore pluggage. This phenomenon was also responsible for the significantly lower decrease in initial rate of carbonation under CO_2 calcination conditions as compared to the limestone.

For both naturally occurring calcium oxide based sorbents the carbonation temperature has no substantial effect on the level of carbonation conversion over repeated calcination / carbonation cycles as it has been shown that the conversion is only related to the calcination conditions.

The effects of major operating parameters such as inlet CaO and feed gas superficial velocities, inlet temperature, and number of calcination / carbonation cycles on the behaviour of the carbonation reaction in a moving bed reactor have been determined. As the CaO feed superficial velocity was increased beyond 0.0010 m/s the increase in bed temperature resulted in a value of $C_{CO_2,eq}$ close to that in the bulk gas stream limiting the rate of carbonation resulting in an incomplete usage of the maximum CaO capture capability. It was determined that the optimal feed gas superficial velocity lies between 3 and 5 m/s to both maximize the CaO conversion while also minimizing the outlet CO_2 gas composition. From this parametric analysis it became evident that one major method for improving the overall efficiency of the process would be to add a cooling jacket (or another cooling system, e.g., tube bundles) around the entrance of the reactor, where the majority of the carbonation takes place. Thus, the feed gas flow rate could be adjusted to obtain any desirable CO_2 outlet composition and thus, eliminating the necessity of high superficial velocities for the convective heat removal.

The following is a list of future work that should be performed to further the understanding of the presence of gasification syngas on the capture of CO_2 via cyclic carbonation / calcination:

- Perform additional TGA experiments where the calcium oxide based sorbents are carbonated under CO_2 without the presence of gasification syngas (CO, H_2, and H_2O) to investigate the effect of steam on the cyclic carbonation conversion.
- Perform tube furnace experiments to quantify the increase in macroporosity / decrease in microporosity over repeated calcination / carbonation cycles as TGA sample sizes are too small for BET N_2 adsorption.
- Perform moving bed reactor experiments to quantify the water-gas shift reaction, by monitoring the outlet concentrations of CO and H_2, and to validate the reactor model.

Nomenclature

a = reaction order defined in Equation 3.14, dimensionless

C_{CO_2} = CO_2 concentration, kmol/m^3

$C_{CO_2,eq}$ = equilibrium CO_2 concentration, kmol/m^3

$C_{CO_2,0}$ = inlet CO_2 concentration, kmol/m^3

C_{pg} = heat capacity of bulk gas, kJ/kmol.K

C_{ps} = heat capacity of CaO, kJ/kmol.K

C_T = total inlet bulk gas concentration, kmol/m^3

d_p = particle diameter, m

d_r = inner diameter of reactor, m

E = activation energy, kJ/mol

f_m = fitting parameter in Equation 2.5, dimensionless

f_w = fitting parameter in Equation 2.5, dimensionless

F_{CO_2} = flowrate of CO_2, kmol/s

h_w = wall-bed heat transfer coefficient, kJ/m^2.s.K

H_{cbn} = reaction heat of CaO carbonation, kJ/kmol

k = apparent rate constant in Equation 3.4, 1/s

k' = random pore model rate constant in Equation 3.2, 1/s

k'' = random pore model rate constant in Equation 3.3, 1/s$^{0.5}$

k_0 = pre-exponential factor in Equation 3.19, mol/m^2.s

k_g = thermal conductivity of bulk gas, kJ/m.s.K

k_s = intrinsic surface rate constant in Equation 3.14, mol/m^2.s.kPa^n

m_{CaCO_3,CO_2} = mass of dolomite after complete calcination of $MgCO_3$, mg

$m_{CaO,b,N}$ = mass of $CaCO_3$ calcines after complete carbonation, mg

$m_{CaO}(0)$ = mass of $CaCO_3$ calcines at time zero, mg

$m_{CaO}(t)$ = mass of $CaCO_3$ calcines at time t, mg

M_{CaO} = molecular weight of CaO, kg/kmol

n = parameter in Equation 3.4, dimensionless

N = number of calcination / carbonation cycles

P = total system pressure, Pa

P_0 = inlet system pressure, Pa

P_{CO_2} = partial pressure of CO_2, atm

$P_{CO_2,eq}$ = equilibrium partial pressure of CO_2, atm

$purity$ = mass fraction of $CaCO_3$ of fresh sorbent, dimensionless

r = reaction rate in Equation 3.10, 1/s

r_0 = reaction rate r at time zero, 1/s

r_{cbn} = rate of CO_2 removal by CaO carbonation, kmol/kg-CaO.s

R = specific rate of reaction in Equation 3.13, 1/s

R_g = gas constant, 8.314×10^{-3}, kJ/mol.K

Re_p = particle Reynolds number, dimensionless

s = slope of the line of best fit in Equation 2.7, dimensionless

S = specific surface area, m^2/g

S_0 = specific surface area at time zero, m^2/g

$slope$ = slope of the least-square regression analysis in Equation 3.9, 1/s

t = time, s

T = temperature, K

T_0 = inlet temperature, K

T_w = reactor wall temperature, K

u_g = bulk gas superficial velocity, m/s

$u_{g,0}$ = inlet bulk gas superficial velocity, m/s

u_s = CaO superficial velocity, m/s

X = fractional carbonation conversion of CaO, dimensionless

$X_{b,N}$ = limited carbonation conversion of CaO for the N^{th} cycle, dimensionless

X_u = ultimate fractional carbonation conversion of CaO, dimensionless

z = axial distance of reactor from inlet, m

Greek Letters

ε = bed void fraction, dimensionless

γ = parameter in Equation 3.24, 1/s

μ = viscosity of bulk gas, Pa.s

ν = volumetric flow rate of bulk gas, m^3/s

ρ_{CaO} = apparent density of CaO particles, kg/m^3

ρ_g = density of bulk gas, kg/m^3

ψ = structural parameter in Equations 3.2 and 3.3, dimensionless

ψ_{CO_2} = parameter in Equation 3.26, $kmol/m^3.s$

References

Abanades, J. C., Alvarez, D., *Conversion Limits in the Reaction of CO_2 with Lime*, Energy and Fuels, 17, 308 (2003).

Abanades, J. C., Alvarez, D., Anthony, E. J., Lu, D., *In Situ Capture of CO_2 in a Fluidized Bed Combustor*, 17th Int. Conf. on Fluidized Bed Combustion, ASME, Jacksonville, FL, ASME, New York (2003).

Abanades, J. C., Anthony, E. J., Alvarez, D., Lu, D., Salvador, C., *Capture of CO_2 from Combustion Gases in a Fluidized Bed of CaO*, A.I.Ch.E. Journal, 50, 1614-1622 (2004).

Baker, E. H., *The Calcium Oxide-Carbon Dioxide System in the Pressure Range 1-300 Atmospheres*, Chem. Soc., 462, 70 (1962).

Bhatia, S. K., Perlmutter, D. D., *Effect of the Product Layer on Kinetics of the CO_2-Lime Reaction*, A.I.Ch.E. Journal, 29 (1), 79-86 (1983).

Borgwardt, R. H., *Calcium Oxide Sintering in Atmospheres Containing Water and Carbon Dioxide*, Ind. Eng. Chem. Res., 28, 493-500 (1989).

Borgwardt, R. H., *Sintering of Nascent Calcium Oxide*, Chem. Eng. Sci., 44, 53-60 (1989).

Curran, G. P., Fink, C. E., Gorin, E., *Carbon Dioxide-Acceptor Gasification Process. Studies of Acceptor Properties*, Adv. Chem. Ser., 69, 141 (1967).

Dennis, J. S., Hayhurst, A. N., *The Effect of CO_2 on the Kinetics and Extent of Calcination of Limestone and Dolomite Particles in Fluidized Beds*, Chemical Engineering Science, 42, 2361-2372 (1987).

Ergun, S., *Fluid Flow through Packed Columns*, Chemical Engineering Progress, 48, 89-94 (1952).

Feyo De Azevedo, S., Romero-Ogawa, M. A., Wardle, A. P., *Modeling of Tubular Fixed Bed Catalytic Reactors: A Brief Review*, Transactions of the Institution of Chemical Engineers, 68 (A), 483-502 (1990).

Gupta, H., Fan, L. S., *Carbonation-Calcination Cycle Using High Reactivity Calcium Oxide for Carbon Dioxide Separation from Flue Gas*, Ind. Eng. Chem. Res., 41, 4035-4042 (2002)

Han, C., Harrison, D. P., *Simultaneous Shift Reaction and Carbon Dioxide Separation for the Direct Production of Hydrogen*, Chemical Engineering Science, 49, 5875-5883 (1994).

Herzog, H., *What Future for Carbon Capture and Sequestration?*, Env. Sci. and Technol., 4, 148A (2001).

Houghton, J. T. T., Meira Filho, L. G., Callander, B. A., Harris, N., Kattenberg, A., Maskell, K., Eds. *Climate Change 1995*, working group I, published for the Intergovernmental Panel on Climate Change, Cambridge University Press: Cambridge, U.K., (1996).

IPCC Special Report, *Carbon Dioxide Capture and Storage – A Special Report of Working Group III of the Intergovernmental Panel on Climate Change*, September (2005).

Jia, L., Hughes, R., Anthony, E. J., Lau, I., *Attrition of Calcined Limestone in Circulating Fluidized-Bed Systems*, Ind. Eng. Chem. Res., *46*, 5199-5209 (2007).

Keeling, C. D., Bacastow, R. B., Whorf, T. P., Mook, W. G., *Evidence for Accelerated Releases of Carbon Dioxide to the Atmosphere Inferred from Direct Measurements of $^{13}C/^{12}C$ Ratio*, Proceedings of the 82nd Annual Meeting of the Air and Waste Management Association, Pittsburgh, PA, Vol. 7, Paper 89-119.2 (1989).

Kikkinides, E. S., Yang, R. T., Cho, S. H., *Concentration and Recovery of CO_2 from Flue Gas by Pressure Swing Adsorption*, Ind. Eng. Chem. Res., 32, 2714-2720 (1993).

Kim, M., Pettersen, J., Bullard, C. W., *Fundamental Process and System Design Issues in CO_2 Vapor Compression Systems*, Process in Energy and Combustion Science, 30, 119-174 (2004).

Kunii, D., Levenspiel, O., *Fluidization Engineering*, Wiley, NY, 480-489 (1969).

Kyaw, K., Kanamori, M., Matsuda, H., Hansatani, M., *Study of Carbonation Reactions of Ca-Mg Oxides for High Temperature Energy Storage and Heat Transformation*, Journal of Chemical Engineering of Japan, 29 (1), 112-118 (1996).

Lee, D. K., *An Apparent Kinetic Model for the Carbonation of Calcium Oxide by Carbon Dioxide*, Chemical Engineering Journal, 100, 71-77 (2004).

Lee, D. K., Baek, I. H., Yoon, W. L., *Modeling and Simulation for the Methane Steam Reforming Enhanced by In Situ CO_2 Removal Utilizing the CaO Carbonation for H_2 Production*, Chem. Eng. Sci., 59, 931-942 (2004).

Li, C., Finlayson, B. A., *Heat Transfer in Packed Beds – A Reevaluation*, Chemical Engineering Science, 32, 1055-1066 (1977).

Li, Z., Cai, N., Huang, Y., Han, H., *Synthesis, Experimental Studies, and Analysis of a New Calcium-Based Carbon Dioxide Absorbent*, Energy & Fuels, 19, 1447-1452 (2005).

Lin, S. Y., Suzuki, Y., Hatano, H., Harada, M., *Developing an Innovative Method HyPr-RING to Produce Hydrogen from Hydrocarbons*, Energy Conversion and Management, 43 (9-12), 1283 (2002).

McCauley, R. A., Johnson, L. A., *Decrepitation and Thermal Decomposition of Dolomite*, Thermochimica Acta, 185, 271-282 (1991).

Rao, A. B., Rubin, E. S., *A Technical, Economic, and Environmental Assessment of Amine-Based CO_2 capture Technology for Power Plant Greenhouse Gas Control*, Environ, Sci. Technol., 36, 4467-4475 (2002).

Reimer, P., Audus, H., Smith, A., *Carbon Dioxide Capture from Power Stations*, IEA Greenhouse R&D Programme: Cheltenhamter, U.K., (2001).

Rofer-DePoorter, C., *Untangling the Water Gas Shift from Fischer Tropsch*, Catalytic Conversions of Synthesis Gas and Alcohols to Chemicals, Plenum Press, NY, 97-128 (1984).

Shih, S. M., Ho, C. S., Song, Y. S., Lin, J. P., *Kinetics of the Reaction of $Ca(OH)_2$ with CO2 at Low Temperature*, Ind. Eng. Eng. Chem. Res., 38 (4), 1316 (1999).

Shimizu, T., Hirama, T., Hosoda, H., Kitano, K., Inagaki, M., Tejima, K., *A Twin Fluid-Bed Reactor for Removal of CO_2 From Combustion Processes*, Trans. I. Chem. E., 77-A, 62 (1999).

Silaban, A., Harrison, P., *High Temperature Capture of carbon Dioxide: Characteristics of the Reversible Reaction between CaO(s) and $CO_2(g)$*, Chemical Engineering Communications, 137, 177-190 (1995).

Silcox, G. D., Kramlich, J. C., Pershing, D. W., *A Mathematical Model for the Flash Calcination of Dispersed $CaCO_3$ and $Ca(OH)_2$ Particles*, Ind. Eng. Chem. Res., 28, 155-160 (1989)

Simbeck, D. R., Korens, N., Biasca, F. E., Vejtasa, S., Dickenson, R. L., *Coal Gasification Guidebook: Status, Applications and Technologies*, EPRI TR-102034, Palo Alto, CA, USA, EPRI, vp (1993).

Stanmore, B. R., Gilot, P., *Review – Calcination and Carbonation of Limestone During Thermal Cycling for CO_2 Sequestration*, Fuel Processing Technology, 86, 1707-1743 (2005)

Sun, P., Grace, J. R., Jim Lim, C., Anthony, E. J., *A Discrete-Pore-Size-Distribution-based Gas-Solid Model and its Application to the CaO + CO_2 Reaction*, Chemical Engineering Science, 63, 57-70 (2008a).

Sun, P., Grace, J. R., Jim Lim, C., Anthony, E. J., *Determination of Intrinsic Rate Constants of the CaO-CO_2 Reaction*, Chemical Engineering Science, 63, 47-56 (2008b).

Szekely, J., Evans, J. W., Sohn, H. Y., *Gas Solid Reactions*, Academic Press, London (1976).

Wang, C., Jia, L., Tan, Y., Anthony, E. J., *Carbonation of Fly Ash in Oxy-Fuel CFB Combustion*, Fuel, *87*, 1108-1114 (2008).

Young, D. A., *Decomposition of Solids*, Pergamon Press, Oxford (1966).